



HAL
open science

**Complexes of the tripodal phosphine ligands
PhSi(XPPh₂)₃ (X = CH₂, O): synthesis, structure
and catalytic activity in the hydroboration of CO₂**

Alicia Aloisi, Jean-Claude Berthet, Caroline Genre, Pierre Thuéry, Thibault
Cantat

► **To cite this version:**

Alicia Aloisi, Jean-Claude Berthet, Caroline Genre, Pierre Thuéry, Thibault Cantat. Complexes of the tripodal phosphine ligands PhSi(XPPh₂)₃ (X = CH₂, O): synthesis, structure and catalytic activity in the hydroboration of CO₂. Dalton Transactions, 2016, 45, pp.14774-14788. 10.1039/c6dt02135b . cea-01369401

HAL Id: cea-01369401

<https://cea.hal.science/cea-01369401>

Submitted on 15 Feb 2019

HAL is a multi-disciplinary open access archive for the deposit and dissemination of scientific research documents, whether they are published or not. The documents may come from teaching and research institutions in France or abroad, or from public or private research centers.

L'archive ouverte pluridisciplinaire **HAL**, est destinée au dépôt et à la diffusion de documents scientifiques de niveau recherche, publiés ou non, émanant des établissements d'enseignement et de recherche français ou étrangers, des laboratoires publics ou privés.

Complexes of the Tripodal Phosphine Ligands PhSi(XPPh₂)₃ (X = CH₂, O): Synthesis, Structure and Catalytic Activity in the Hydroboration of CO₂†

Alicia Aloisi, Jean-Claude Berthet,* Caroline Genre, Pierre Thuéry and Thibault Cantat*

NIMBE, CEA, CNRS, Université Paris-Saclay, CEA Saclay 91191 Gif-sur-Yvette, France.

Keywords: Tripodal ligands, Phosphorus ligands, Iron, Cobalt, Copper, Carbon dioxide reduction, Hydroboration.

Abstract: The coordination chemistry of the Fe²⁺, Co²⁺ and Cu⁺ ions was explored with the triphosphine and triphosphinite ligands PhSi{CH₂PPh₂}₃ (**1**) and PhSi{OPPh₂}₃ (**2**), so as to evaluate the impact of the electronic properties of the tripodal phosphorus ligands on the structure and reactivity of the corresponding complexes. The synthesis and characterization of the complexes [Fe(κ³-PhSi{CH₂PPh₂}₃)(MeCN)₃][OTf]₂ (**3**) (OTf = O₃SCF₃), [Fe(κ³-PhSi{OPPh₂}₃)(MeCN)₃][OTf]₂ (**3'**), [Co(κ²-PhSi{CH₂PPh₂}₃)Cl₂] (**4**), [Co(κ³-PhSi{OPPh₂}₃)Cl₂] (**4'**), [Cu(κ³-PhSi{CH₂PPh₂}₃)Br] (**5**) and [Cu(κ³-PhSi{OPPh₂}₃)I] (**5'**) were carried out. The crystal structures of **3**, **3'**, **4**, **4'**, and of the solvates **5**·3THF and **5'**·THF are reported. Complexes **3–5'** were shown to promote the catalytic hydroboration of CO₂ with (9-BBN)₂ (9-BBN = 9-Borabicyclo[3.3.1]nonane). While the iron and cobalt complexes of the triphosphine **1** are more active than the analogous complexes with **2**, the opposite trend is observed with the copper catalysts. Overall, the copper catalysts **5** and **5'** are both more reactive and more selective than the Fe and Co catalysts, enabling the formation of the acetal H₂C(OBBN)₂ with a high molar ratio of H₂C(OBBN)₂:CH₃OBBN up to 92:8.

† CCDC reference numbers 1481874–1481881. For crystallographic data in CIF or other electronic format see DOI:

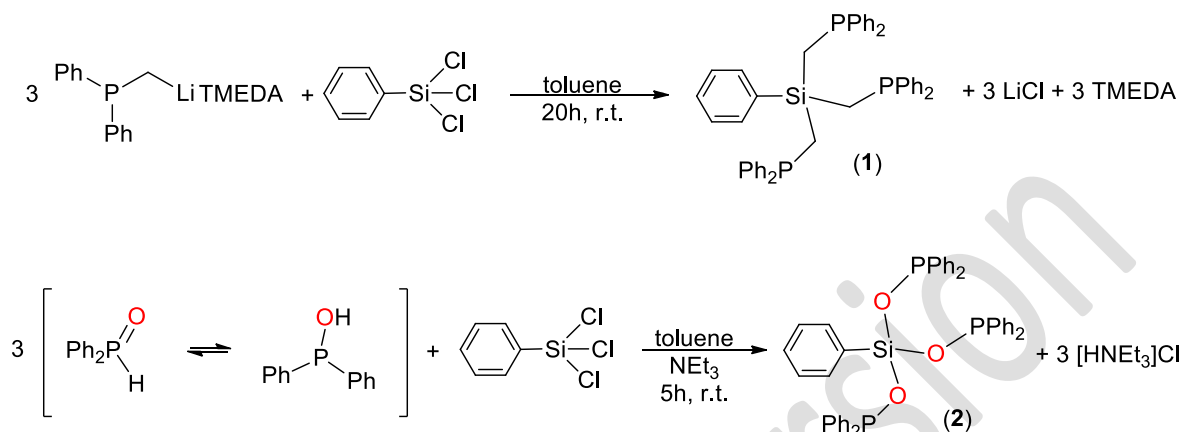
Introduction

Tripodal ligands play a major role in transition metal chemistry, as they increase the stability of their complexes and enable a fine control of the reactivity at the metal center through their steric and electronic properties and their specific coordination geometry. Within tripodal ligands, a few triphosphines have been utilized so far in coordination chemistry and catalysis and, among them,¹ triphos ($\text{MeC}(\text{CH}_2\text{PPh}_2)_3$) has attracted considerable attention over the last years, being a valuable ligand for a number of late transition metals (with *ca* 700 crystal structures). The ability of triphos to stabilize low metal oxidation states and to adopt both κ^2 - and κ^3 -coordination modes has led to widespread and successful applications in catalysis, including CO_2 hydrogenation, disproportionation of formic acid and reduction of amides.^{2,3,4,5,6,7} The efficiency of catalytic reactions is generally strongly influenced by the nature of the ancillary ligand. Because small changes within a ligand series, such as the pendant alkyl chains or the nature and/or the position of the linking groups, can induce different outcomes in a catalytic reaction, variations on the triphos backbone have been reported. Tripodal molecules such as PP_3 ($\text{PP}_3 = \text{P}\{\text{CH}_2\text{PR}_2\}_3$), $\text{N}\{\text{CH}_2\text{PR}_2\}_3$, $\text{R}'\text{Si}\{\text{CH}_2\text{PR}_2\}_3$, etc. have been synthesized along with their coordination complexes.^{8,9,10} In particular, $\text{R}'\text{Si}(\text{CH}_2\text{PR}_2)_3$ ligands, featuring an organosilane linker, have been investigated and a number of their complexes exist with Ti,^{11,12,13,14} V,^{13,15,16,17} Cr,¹⁸ Fe,^{1,19,20,21,22,23} Cu,²⁴ Nb,^{2,16,25} Mo,^{26,27} Ru,^{1,24,28,29,30,31} Rh,²⁴ Pd,²⁴ Ta,^{2,16,32} W,³³ Os¹ and Pt.²⁴ Surprisingly, oxygen analogues of formula $\text{RSi}(\text{OPR}'_2)_3$ have remained elusive so far and, to our knowledge, only a single transition metal complex, *eg* $[\text{Mo}(\text{MeSi}\{\text{OPOMe}_2\}_3)(\text{CO})_3]$, has been crystallographically characterized.³⁴

In this contribution we report the use of $\text{PhSi}(\text{CH}_2\text{PPh}_2)_3$ (**1**) and its phosphinite derivative $\text{PhSi}(\text{OPPh}_2)_3$ (**2**) in the coordination chemistry of first-row transition metals, namely iron(II), cobalt(II) and copper(I) ions. The syntheses, NMR characterizations and crystal structures of pairs of complexes with the ligands **1** and **2** are detailed. To establish the influence of replacing the phosphines groups in **1** with phosphinites, the catalytic activity of the complexes was explored in the hydroboration of CO_2 with (9-BBN)₂. Because CO_2 is a stable chemical waste, its selective multi-electron reduction under mild-conditions remains a challenge^{35,36} and an ideal platform to establish structure/activity relationships for analogous catalysts.

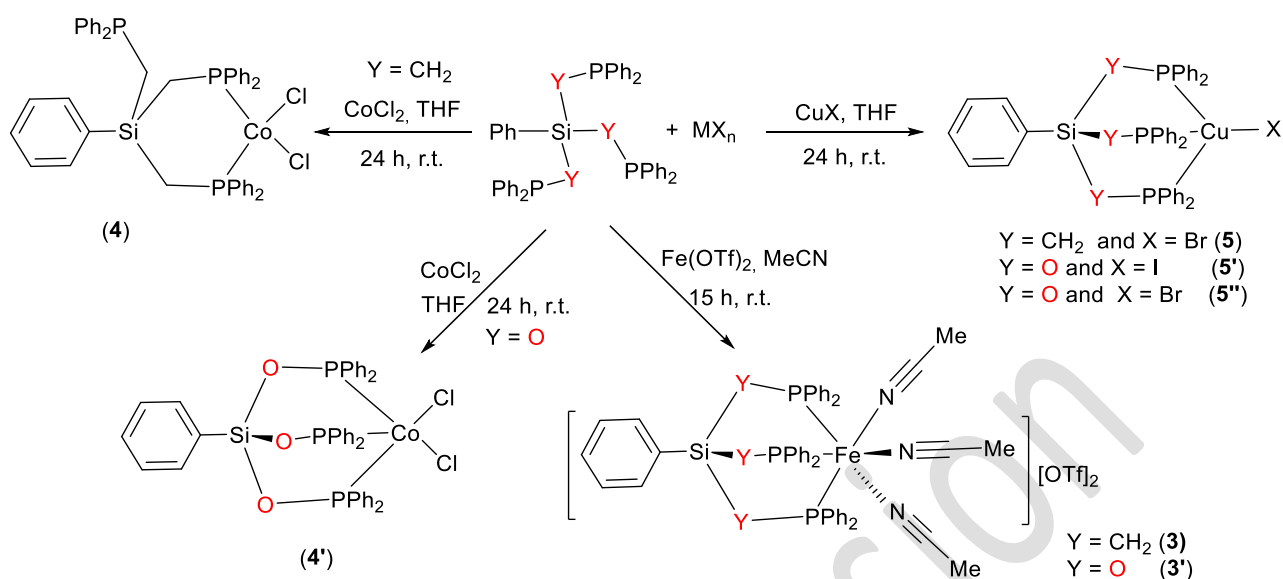
Results and discussion

Synthesis of ligands 1 and 2



Scheme 1: Synthesis of the $\text{PhSi(XPPH}_2)_3$ ligands ($\text{X} = \text{O, CH}_2$).

The syntheses of triphosphine $\text{PhSi(CH}_2\text{PPh}_2)_3$ (**1**) and its phosphinite analogue $\text{PhSi(OPPh}_2)_3$ (**2**) are described in Scheme 1. Ligand **1** was obtained in a good 75 % yield, from a published protocol,^{1,37,38} by reacting a toluene solution of $\text{Ph}_2\text{PCH}_2\text{Li(TMEDA)}$ with PhSiCl_3 in a 3:1 molar ratio. The new species **2** was prepared by analogy with the synthetic procedures reported for the phosphite esters $\text{RSi(OP}\{\text{OR}'\})_3$ ($\text{R} = \text{Ph, Me}$; $\text{R}' = \text{OMe, OEt}$), by mixing PhSiCl_3 with 3 equivalents of $\text{Ph}_2\text{P(=O)H}$. $\text{Ph}_2\text{P(=O)H}$ is involved in an equilibrium with the phosphorus(III) derivatives $\text{Ph}_2\text{P-OH}$ and it readily adds to the chlorosilane, in the presence of NEt_3 as a base, in toluene.^{34, 39-40} After 5 h at room temperature, the solution was filtered to remove the HNEt_3Cl deposit and **2** was obtained pure as a colorless oil, after vacuum drying (88 % yield). Compound **2** was characterized by its ^1H , ^{13}C and $^{31}\text{P}\{^1\text{H}\}$ NMR spectra in d_8 -THF. **2** exhibits a singlet at δ_{P} 100.93 for the P atoms which is shifted downfield in comparison to the chemical shift of -20.21 ppm in THF (-23.59 in benzene) for **1** (vs -27.3 ppm for triphos (toluene, -40°C)).^{1,41} These δ_{P} values for **1** and **2** fall in the range of classical phosphine and phosphinite groups, respectively. Importantly, the thermal stabilities of **1** and **2** strongly differ. Whereas a refluxing solution of **1** in benzene shows no sign of decomposition after 24 h, **2** rapidly degraded under the same conditions to a large number of unidentified phosphorus species.



Scheme 2: Synthesis of the Fe²⁺, Co²⁺ and Cu⁺ complexes with the Ph-Si(YPPH₂)₃ ligands (Y = O, CH₂).

Formation of iron complexes 3 and 3'

Treatment of FeCl₂ with RSi(CH₂PPh₂)₃ (R = Ph, *i*-Pr)¹ or the less sterically demanding ligands R'Si(CH₂PMe₂)₃ (R' = *t*Bu, Me)^{20, 22} has been previously reported, both in THF and CH₂Cl₂. In these weakly polar solvents, the colorless paramagnetic complexes [Fe(κ²-RSi{CH₂PPh₂})₃Cl₂] (R = Ph, *i*-Pr)¹ or the purple, diamagnetic cationic [(Fe(κ³-RSi{CH₂PMe₂})₃)₂(μ-Cl)₃][Cl]²⁰ complexes were formed. The pink iron(II) monocationic derivatives [Fe(κ³-RSi{CH₂PMe₂})(μ-Cl)(Me₂P(CH₂)_nPMe₂)] [Cl] (n = 1, 2)^{22, 23} were also obtained from the dinuclear species by addition of dmpe or dmpm (dmpe = dimethylphosphinoethane; dmpm = dimethylphosphinomethane).²² These results provide a trend where the tridentate coordination mode of the RSi{CH₂PR'₂})₃ ligands always affords diamagnetic and colored iron complexes, whereas colorless and paramagnetic derivatives are obtained with κ²-coordinated ligands.

The polarity of the solvent and the nature of the X ligand in the FeX₂ salt were found to influence the coordination mode (bidentate vs tridentate) of the RSi{CH₂PR'₂})₃ triphosphine ligands. In addition, these parameters govern the crystallization of the complexes, which are obtained either in their neutral or cationic form. We thus considered the reaction of **1** and **2** with Fe(OTf)₂ and acetonitrile (ε = 37.5 vs 7.5 for THF), aiming at preparing discrete cationic species with octahedral geometry. Reaction

of **1** and **2** with Fe(OTf)₂ in acetonitrile afforded orange (Y = O) and red (Y = CH₂) solids, which crystallized readily in acetonitrile as **3** and **3'**, respectively, in moderate yields (55 and 52%, respectively). **3** and **3'** underwent partial desolvation of the acetonitrile ligands during vacuum drying, and elemental analyses and ¹H NMR data collected for the resulting solids suggested a coordination of 2 to 3 acetonitrile molecules per iron ion. The iron complexes are soluble in THF yet insoluble in non-polar solvents. **3** and **3'** were characterized by ¹H, ¹³C and ³¹P{¹H} NMR spectroscopy, from their acetonitrile solutions. Characteristic ³¹P{¹H} resonance for **3** is a unique singlet at 30.15 ppm, shifted downfield with respect to the free ligand **1** (-20.21 ppm). A similar trend is noted for **3'**, which ³¹P{¹H} spectrum features a singlet at δ_P 147.9, shifted +47 ppm downfield from the free ligand **2**. The NMR data of **3** are similar to those observed for [Fe(PhCH₂C{CH₂PPh₂})₃(NCMe)₃][BF₄]₂ (δ_P 33.2) and [Fe(triphos)(NCMe)₃][BF₄]₂ (δ_P 32.3).^{42,43}

Large red and orange crystalline platelets of **3** and **3'** were obtained by layering diethyl ether on an acetonitrile solution of the compounds. Both complexes crystallized as discrete cation–anion pairs and views of the cations of **3** and **3'** are shown in Figure 1, respectively, while selected bond lengths and angles are gathered in Table 1. **3** and **3'** are isostructural with the iron ion lying in a distorted octahedral environment, formed by three acetonitrile molecules and the κ³-coordinated tripodal ligand (**1** or **2**). The structures are reminiscent to that of the related [Fe(κ³-MeSi{CH₂PPh₂})₃(NCMe)₃][BF₄]₂ complex, reported during the course of the present study,²¹ and to that of [Fe(κ³-RC{CH₂PPh₂})₃(NCMe)₃][BF₄]₂ (R = Me, PhCH₂).⁴² The mean Fe–P and Fe–N distances in **3** [2.308(11) Å and 1.958(4) Å] compare well with those reported in [Fe(κ³-MeSi{CH₂PPh₂})₃(NCMe)₃][BF₄]₂ [2.317(7) and 1.966(2) Å]²¹ or [Fe(κ³-triphos)(NCMe)₃][BF₄]₂ [2.27(1) and 1.953(6) Å].⁴⁴ While the mean Fe–N bond lengths are similar in **3** and **3'** [1.962(4) Å for **3'**], the Fe–P distances in **3'** are notably shorter averaging 2.255(8) Å. This contraction is in agreement with the greater 3s character in the phosphorus lone pair of a phosphinite ligand, compared to a phosphine. The P–Fe–P and N–Fe–N bite angles average 92.7(8)° and 85.3(15)° in **3**, and 91.1(18)° and 86.2(14)° in **3'**, whereas these values reach 88(2)° and 85(1)° in [Fe(κ³-MeC{CH₂PPh₂})₃(NCMe)₃][BF₄]₂ and 92(2)° and 84.4(7)° in [Fe(κ³-MeSi{CH₂PPh₂})₃(NCMe)₃][BF₄]₂.

Formation of the cobalt complexes **4** and **4'**

Cobalt(II) chloride reacted readily with **1** in THF to afford a blue solution from which complex **4** was isolated as a solid (49 % yield), after several washings with pentane. Treating a THF solution of CoCl₂ with **2** yielded a red solution from which **4'** was isolated as a red solid (36 % yield). Paramagnetism of the 3d⁷ Co²⁺ ion impeded any NMR characterization and the compounds were characterized by X-ray diffraction and elemental analyses. Blue crystals of **4** and dark red crystals of **4'** were obtained by slow diffusion of pentane into a THF and a dichloromethane solution of the complexes, respectively. These distinct colors suggest different coordination geometries around the Co²⁺ ion in **4** and **4'**. It is well established that tetrahedral Co²⁺ complexes are generally blue, while they are pink-red when the metal ion adopts an octahedral configuration.⁴⁵ In fact, within the triphos series, [Co(triphos)Cl₂] provided blue solutions in agreement with a four coordinate [Co(κ²-triphos)Cl₂] structure. Nevertheless, it was isolated as a red five coordinate [Co(κ³-triphos)Cl₂], in the solid state.⁴⁵ The increased stability of **4** with respect to [Co(κ²-triphos)Cl₂] evidences the influence of the Si versus the C atom at the apex position of tripodal ligands. The control of the coordination behavior is likely due to small interplays of steric tension at the C–E–C (E = Si, C) angles. This finding is in agreement with the recent results obtained by Apfel *et al.* on the coordination behavior of the homologous RSi{CH₂PPh₂}₃ (R = Me, Ph) and triphos ligands with FeCl₂. The authors indeed concluded, from titration experiments, that MeSi{CH₂PPh₂}₃ binds FeCl₂ more strongly than triphos in acetonitrile.^{21, 45}

Views of complexes **4** and **4'** are provided in Figure 2, respectively, and selected bond lengths and angles are listed in Table 1. X-ray diffraction confirmed a tetrahedral environment for the Co²⁺ ion in **4** and a distorted square pyramidal coordination geometry in **4'**. In the latter complex, the base is defined by the two halides, P2 and P3 (rms deviation 0.018 Å) while P1 is at the vertex of the pyramid. The metal ion lies inside the pyramid, 0.4372(5) Å above the base and the sum of the ligand-Co-ligand angles in the mean base is 351.14°. The distinct coordination environments in **4** and **4'** are in line with the different electron donating properties of ligands **1** and **2**. Because phosphinite ligands P(OR)₂ are less electron donating than phosphines, CoCl₂ preferentially accommodates ligand **2** in a tridentate manner while κ²-coordination with

the more electron rich triphosphine **1** is favored, resulting in the formation of the four-coordinate species **4**.

Within each complex, the two Co–Cl bond lengths differ by less than 0.03 Å, thus confirming the neutral nature of these species. The Co–Cl distances are shorter in **4** than in **4'**, which reflects the lower coordination number at the Co²⁺ ion in **4**. In addition, Co–P distances in **4** are ca 0.12 Å longer than in **4'**, with average values of 2.3483(6) and 2.22(4) Å in **4** and **4'**, respectively. These structural features are consistent with a chelating effect resulting in a stronger metal-ligand interaction in **4'** and the increased 3s character of the P lone pairs in **2**. The Cl–Co–Cl angle is strongly related to the steric environment of the metal ion. A decreasing coordination number allows the Cl–Co–Cl angle to expand from 88.69(3)° in the five-coordinate complex **4'** to 121.73(4)° in the four-coordinate species **4**. The P–M–P angles in the tridentate MeSi(YPPH₂)₃ (Y=CH₂, O) ligands are unexceptional and quite similar in the iron and cobalt complexes.

Formation of the copper complexes **5**, **5'** and **5''**

Addition of CuBr to a THF solution of **1** afforded [Cu(κ^3 -PhSi{CH₂PPh₂}₃)Br] (**5**), after 24 h reaction at room temperature and washings with pentane. Repeating the same procedure with **2** and CuX (X= I, Br), [Cu(κ^3 -PhSi{OPPh₂}₃)I] (**5'**) and [Cu(κ^3 -PhSi{OPPh₂}₃)Br] (**5''**) could be isolated in good 88 and 82 % yields, respectively. The ¹H, ¹³C and ³¹P{¹H} NMR spectra recorded at 21°C are consistent with complexes having a C₃ symmetry for the three complexes, which was confirmed by X-ray diffraction analyses. Elemental analyses were carried out on the bromide complexes and, because [Cu(κ^3 -PhSi{OPPh₂}₃)Br] could not be crystallized, its iodide counterpart **5'** was further considered in this work. Crystals of the adducts **5**·3THF and **5'**·THF were grown by diffusion of pentane into THF solutions of **5** and **5'**.

The ³¹P{¹H} NMR spectra of **5** and **5'** in dichloromethane at 21°C (Figure 3) exhibit a quartet centered at –33 and + 80 ppm, respectively. A *J*_{P–Cu} coupling constant of 860 Hz is measured for **5'** while the ³¹P{¹H} NMR spectrum of **5** exhibits two nearly superimposed quartets related to the phosphorus coupling with each copper isotope (*J*_{P–63Cu} ~ 860 Hz, *J*_{P–65Cu} ~ 900 Hz). Classically, the ³¹P{¹H} NMR spectra of copper-

phosphine complexes present broad signals and the coupling between the ^{31}P and the two ^{63}Cu and ^{65}Cu isotopes is rarely observed in solution because the isotopes of copper are both quadrupolar nuclei.⁴⁶ In fact, the relaxation rate of quadrupolar nuclei is higher in solution than in the solid state and fluxional behaviors such as ligands exchanges might occur in solution, thereby precluding the observation of fine NMR structures. The observation of P–Cu coupling for **5** and **5'** might point to a strong coordination of the tripodal ligands to the Cu^+ ion and a highly symmetric structure that decreases the electric field gradient at the tetrahedral center, thus reducing the quadrupolar relaxation rate⁴⁷. On the contrary, the $^{31}\text{P}\{^1\text{H}\}$ NMR spectrum of **5''** in THF at 21°C shows a very broad signal at +81 ppm (Fig. S13), indicative of a stronger electric field gradient induced by the combination of a bromide and phosphinite ligand.

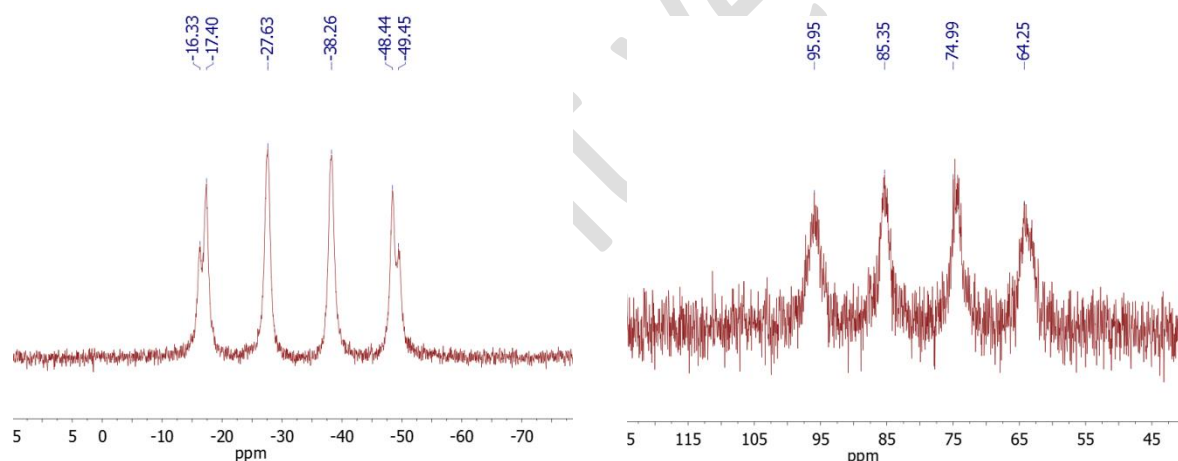
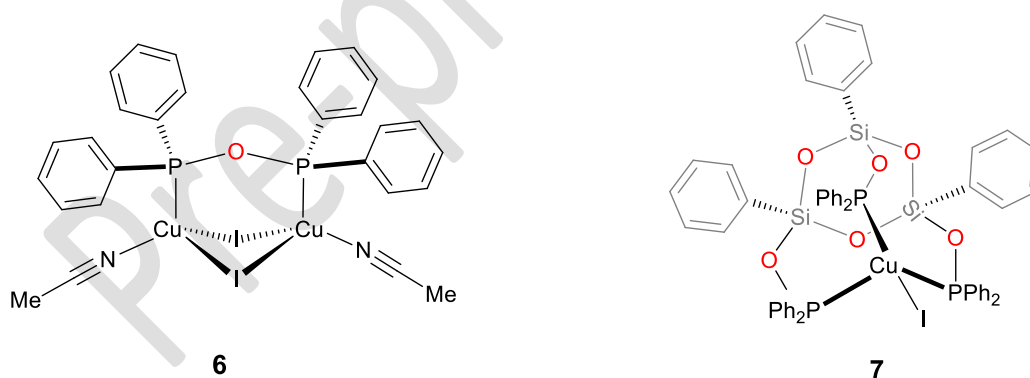


Figure 3: $^{31}\text{P}\{^1\text{H}\}$ NMR spectra of **5** (left) and **5'** (right) in $d_2\text{-CH}_2\text{Cl}_2$ at 21°C.

Although decomposition of the free ligand **2** was noted at 60°C, no product could be identified from crude THF solutions. It is noteworthy that heating for several hours a suspension of CuI or CuCl_2 and **2** in refluxing THF or MeCN also led to the decomposition of the triphosphinite framework. Layering the crude MeCN or THF solution with diethyl ether or pentane, respectively, resulted in the deposition of colorless crystals of the complexes $[\text{Cu}_2(\text{Ph}_2\text{POPPh}_2)_2(\text{NCMe})_2] \cdot (\text{MeCN})$ (**6-MeCN**) or $[\text{Cu}(\text{Ph}_3\text{Si}_3\text{O}_3\{\text{OPPh}_2\}_3)\text{Cl}]$ (**7**). Complex **6** is a dimeric copper(I) complex featuring a $\text{Ph}_2\text{POPPh}_2$ diphosphoxane ligand (Scheme 3). Metal complexes of diphosphoxane

ligands $R_2P-O-PR_2$ are scarce in coordination chemistry and only a fistful of compounds have been crystallographically characterized, such as $M(CO)_4(PPh_2POPPh_2)$ ($M = Mo, Cr$)^{48,49} $[RuCl_2(Ph_2PO_2PPh_2)(PPh_3)(\{Ph_2PO_2\}_2C_2H_4)]$,⁵⁰ or $[Pt_3(PPh_2POPPh_2)(PPh_2)(C_6F_5)_2]$.⁵¹ These examples were often obtained inadvertently, with the P–O–P fragments resulting from the evolution of R_2POH and/or $R_2(O=P)-PR_2$ molecules due to isomerisation of P=O bonding in the presence of M^{2+} ions (Cu, Co...).⁵²⁻⁵⁴ Recently Cu(I) and Cu(II) salts were also found to selectively catalyse the dehydrogenative coupling of $R_2P(=O)H$ molecules to $R_2(O=P)-O-R_2P(=O)$ derivatives, under aerobic conditions.⁵⁵ Here, the Ph_2POPPh_2 ligand in **6** might derive from degradation of **2** due to reaction with adventitious traces of water, after prolonged heating. They would regenerate the phosphinous acid Ph_2POH and its evolution toward Ph_2POPPh_2 .^{55,49,56} Complex **7** presents the coordination of a novel type of triphosphinite ligand in which the PPh_2 moieties are linked through a $[PhSiO]_3$ unit, similar to a silsesquioxane arrangement (Scheme 3). To our knowledge, such an arrangement is unknown and reminiscent of mesitylene based tripodal phosphorus ligands used to form mono and oligomeric assemblages with a variety of *d* and *f* metal ions.⁵⁷⁻⁶⁴ Although ligand **2** is sensitive to temperature, it is notable that its complexes (e.g. **3'**, **4'**, **5'** and **5''**) are more robust and solutions of the complexes in THF show no sign of decomposition after 24 h at 60°C.



Scheme 3: Complexes **6** and **7** obtained from degradation of ligand **2**

Views of the complexes **5**, **5'**, **6** and **7** are given in Figures 4-6, respectively, and selected bond lengths and angles are listed in Table 2. Complexes **5** and **5'** comprise a four-coordinate Cu^+ ion, coordinated to three phosphorus atoms and one terminal halide ion, so that the copper environment can be viewed as distorted trigonal pyramidal, with the P atoms defining the base. The Cu–X ($X = Br, I$) and mean Cu–P

bond lengths [2.4137(12) and 2.285(4) Å for **5**; 2.5491(3) and 2.276(2) Å for **5'**] are unexceptional and fall in the range of the four-coordinate complexes $\text{Cu}(\kappa^3\text{-triphos})\text{Br}$ [2.3983(15) Å and 2.286(6) Å],⁶⁵ $\text{Cu}(\kappa^3\text{-N}\{\text{CH}_2\text{PPh}_2\}_3)\text{Br}$ [2.4965(13) Å and 2.304(4) Å],⁶⁵ $\text{Cu}(\text{PMePh}_2)_3\text{Br}$ [2.507(2) Å and 2.282(9) Å]⁶⁶ and $[\text{Cu}(\kappa^2\text{-dppe})(\mu\text{-}\kappa^1\text{-dppe})\text{I}]$ [2.623(1) and 2.30(2) Å].⁶⁷ The averages for the P–Cu–P and P–Cu–X angles, respectively 100.6(12) and 117(2)° in **5** and 96.55(9) and 120.5(18)° in **5'**, are quite distinct and reflect noticeable deviation from an ideal tetrahedral geometry. These angles are similar to those found in $\text{Cu}(\kappa^2\text{-triphos})\text{Br}$.¹⁸ In all the complexes **3**, **3'**, **4**, **4'**, **5** and **5'**, the Si–O and Si–CH₂ distances are insensitive to the nature of the metal ions and the coordination mode of the ligand.

Complex **6**, $[\text{Cu}(\mu^2\text{-I})_2(\text{NCMe})]_2(\mu^2\text{-(Ph}_2\text{POPPh}_2))$, crystallizes as a solvate with a single acetonitrile molecule in the cell and it presents a two-fold axis of symmetry, defined by the O1 atom and the center of the Cu---Cu fragment. The Cu₂I₂ core adopts a butterfly shape with the I[−] atoms at the wingtips. The two iodide ions and the Ph₂POPPh₂ ligands are bridging and one acetonitrile molecule completes the coordination sphere of the metal ion which is in a pseudo-tetrahedral environment with a mean ligand–Cu–ligand angle of 109(7)°, close to the ideal value. The average Cu–I bond length of 2.701(7) Å is close to mean values in the 4-coordinate phosphite and phosphine derivatives $[\text{Cu}(\mu^2\text{-I})_2(\text{P}\{\text{OPh}\}_3)(\text{NCMe})]_2$ [2.65(2) Å]⁶⁸ and $[\text{Cu}(\mu^2\text{-I})(\text{NCMe})](\mu^2\text{-(C}_{20}\text{H}_{12}\text{O}_2\text{SP})_2\text{NPh})$ [2.68(4) Å].⁶⁹ The Cu---Cu distance of 2.8024(5) Å is classical and equals the sum of the Van der Waals radii (2.80 Å).^{70,71} It is similar to that found in the cationic dimers $[\text{Cu}(\mu^2\text{-dcpm})(\text{NCMe})]_2[\text{BF}_4]_2$ [2.809 Å] (dcpm = bis(dicyclohexylphosphino)methane)⁷² or $[\text{Cu}(\mu^2\text{-Ph}_2\text{P}(\text{CH}_2)_2\text{PPh}_2)(\text{NCMe})]_2[\text{PF}_6]_2$ [2.873 Å].⁷³ The corresponding distance in the twofold bridged dinuclear complex $[\text{Cu}(\mu^2\text{-X})(\text{NCMe})]_2(\mu^2\text{-(R}_2\text{P})_2(\text{N-C}_6\text{H}_4\text{-N})_2(\text{R}_2\text{P})_2)[\text{Cu}(\mu^2\text{-X})(\text{NCMe})]_2$ ⁷⁴ are notably shorter [X = Cl, Br, I ; 2.6893(4), 2.7177(8) and 2.6906(8) Å, respectively]. Such Cu(I)---Cu(I) distances vary considerably for ligand-supported Cu---Cu bonding interactions and contact distances as short as 2.35 Å have been reported.⁷²

Complex **7** crystallizes in the cubic space group *Pa*-3. The environment of the Cu⁺ atom is best described as distorted tetrahedral with bonding to three phosphorus atoms of the novel Ph₃Si₃O₃{OPPh₂}₃ ligand and one chloride anion. The line passing by the

centroid of the cyclic Si₃O₃ fragment and the Cu and Cl atoms is a three-fold axis of symmetry and the Cu atom is at a distance of 3.64 Å from the centroid of the Si₃O₃ ring. The Cu1–Cl1 and Cu1–P1 bond lengths of 2.3022(15) and 2.2550(8) Å, respectively, can be compared to those found in the other 4-coordinate complexes [Cu(κ^3 -triphos)Cl] [2.260 and 2.292(7) Å]⁷⁵ and [Cu(PPh₃)₃Cl] [2.347 and 2.318(1) Å];⁷⁶ the Cu–P bond length is also similar to those measured in **5** and **5'**.

Catalytic hydroboration of CO₂ with **3**, **3'**, **4**, **4'**, **5** and **5'**

Having in hand a series of first row transition metal complexes, namely **3**, **3'**, **4**, **4'**, **5** and **5'**, their catalytic properties were explored in the field of CO₂ transformation. CO₂ conversion is currently dominated by non-redox processes that enable the functionalization of CO₂ to carbonates, carbamates and urethanes.^{35,36, 77-78,35, 79,80} Recent progresses have enabled the coupling of CO₂ and epoxides to either cyclic or polymeric carbonates, with a high regio- and stereoselectivity and using earth abundant metal catalysts.⁸¹⁻⁸⁶ These methods are progressively turning into efficient technologies and some of them are currently under pilot development.^{80, 87} In contrast to functionalization strategies, the reduction of CO₂ offers an access to more energetic C₁ products such as formic acid, carbon monoxide or methanol, with carbon atoms at the +II and –II oxidation states.^{36, 77-78,64a,68,88} So far, the electro-reduction of CO₂ is mostly limited to two electrons processes with the formation of HCOOH and CO, whereas the production of methanol by electrolysis still suffers from low Faraday yields.⁸⁹⁻⁹³ Hydrogenation methodologies nicely supplement electrolysis and, for example, CO₂ hydrogenation to methanol can be promoted by solid copper-based catalysts, on the industrial scale.^{80, 87-88} In solution, several molecular catalysts have been proposed for the hydrogenation of CO₂ to formic acid or methanol.^{6, 94-97} So far, only a single molecular catalyst has been reported for the reduction of CO₂ to methanol with H₂, based on ruthenium(II) complex supported by the triphos ligand.⁹⁶ Replacing H₂ with hydrosilanes (R₃SiH) or hydroboranes (R₂BH) enables the use of extremely mild reaction conditions for the reduction of CO₂, because the Si–H and B–H functionalities are polarized and more reactive.⁹⁸⁻¹¹⁰ While hydrogenation of CO₂ imposes the use of metal catalysts working at high temperature (>120 °C) and high pressure (>80 bars), hydrosilylation and hydroboration reactions can be performed under ambient conditions (25 °C, <1 bar CO₂) with first row transition metal or metal

free catalysts. These advantages have been exemplified with the recent development of novel diagonal reactions⁷⁹ leading to the reductive functionalization of CO₂ to formamides, formamidines, methylamines, etc.¹¹¹ Although hydrosilanes and hydroboranes will not be suitable for large scale applications in the short run – because of cost and atom efficiency – they offer an increased chemoselectivity in the reduction of CO₂. In particular, C⁰ derivatives such as acetals and amins have been successfully obtained from CO₂ and hydrosilanes or hydroboranes, while the corresponding formaldehyde state has been elusive so far when H₂ is utilized in the reduction of CO₂.^{112,113}

Ligands **1** and **2** are synthetic derivatives of the well-known tripodal triphos and PP₃ (tris[2-(diphenylphosphino)ethyl]phosphine) ligands, which d transition metal (Ru, Fe, Cu, etc.) complexes have been successfully utilized in hydrogen transfer catalysis,^{6, 114} specifically for the reduction of carbonyl compounds and CO₂ or the generation of H₂ from formic acid.^{115,116,117} The catalytic activity of **3**, **3'**, **4**, **4'**, **5** and **5'** was thus evaluated in the hydroboration of CO₂ so as to determine the influence of the metal ion and the electronic nature of the ligand in this model reaction.

Exposing an acetonitrile solution of 9-BBN and 1.5 mol% **5** to an excess CO₂ (1 bar) resulted in the formation of the boryl acetal H₂C(OBBN)₂ and methoxyborane CH₃OBBN products in 32 and 13 % yield, after 24 h at 25 °C (Entry 3 in Table 4). This result corresponds to a conversion of 45 % of the B–H functionalities and to an H₂C(OBBN)₂/CH₃OBBN molar ratio of 71:29. Interestingly, the triphosphinite complex **5'** exhibits a higher catalytic activity and a conversion of 69 % is reached after only 4 h at 25 °C, while full completion is noted after 17 h (Entries 4 and 5 in Table 4). **5'** is also more selective than **5** and provides a selectivity of H₂C(OBBN)₂/CH₃OBBN= 80:20 at full conversion (92:8 after 4 h). Complexes **5** and **5'** are only the second examples of copper complexes able to catalyze the hydroboration of CO₂. In 2013, Shintani and Nozaki indeed reported the use of copper(I) N-heterocyclic carbene (NHC) complexes able to reduce CO₂ to formoxyboranes HCOOBR₂ at low temperature (35 °C).¹¹⁸ Importantly, whereas (NHC)CuX (X= OCHO, *O**t*-Bu) catalysts selectively yield formate derivatives, **5** and **5'** converge directly to the acetal product showing that the hydroboration of the latter to the methoxyborane is kinetically limiting. This selectivity is rather unusual and has been described, so far, only with (dmpe)₂FeH₂, as reported recently by the group of Sabo-Etienne and Bontemps.¹¹³

In contrast, the iron and cobalt complexes **3**, **3'**, **4** and **4'** show no catalytic activity in the hydroboration of CO₂ with 9-BBN at room temperature and raising the reaction temperature to 60 °C is needed to observe the reduction of CO₂. Using the triphosphine iron complex **3**, 45 % of the hydroborane is converted after 24 h at 60 °C to a 19:81 mixture of H₂C(OBBN)₂ and CH₃OBBN (Entry 10 in Table 4). Interestingly, the triphosphinite analogue **3'** displays a lower catalytic activity and a conversion of only 3 % under identical conditions (Entry 12). The cobalt complexes **4** and **4'** exhibit a slightly enhanced reactivity, with a conversion of 63 and 6 % with **4** and **4'**, respectively, after 24 h at 60 °C. The iron and cobalt complexes thus differ from copper catalysts **5** and **5'** as they show a lower activity in hydroboration for the phosphinite derivatives (**3'** and **4'**) than the phosphine complexes (**3** and **4**). In addition, different selectivities are observed between the two groups of catalysts. Whereas iron and cobalt complexes **3**, **3'**, **4** and **4'** produce the methoxyborane as a major product (with a H₂C(OBBN)₂/CH₃OBBN molar ratio of ca. 20:80), even at low conversions. The selectivity of **3** and **4** toward the methoxyborane is expectedly more pronounced with an excess of (9-BBN)₂ (Entries 20-23), because CH₃OBBN is the thermodynamic product. The copper complexes **5** and **5'** favor the formation of the C⁰ product (H₂C(OBBN)₂/CH₃OBBN ratio of ca. 80:20), which is only slowly converted to the methoxide level. These trends reveal that different mechanisms are at play in the metal-catalyzed hydroboration of CO₂. Presumably, the copper complexes act as Lewis acids in this transformation and their catalytic activity is enhanced when the Cu⁺ ion is coordinated to the less electron donating ligand **2**. These different mechanisms also translate into different reactivities of the catalysts in the presence of a high concentration of hydroborane. Indeed, while catalysts **3** and **4** are more active with an excess hydroborane, doubling the initial quantity of 9-BBN poisons **5'** which Turn Over Frequency (TOF) drops from 11.5 to 1.6 h⁻¹ (Entries 19–23 in Table 4).

To the best of our knowledge, complexes **4** and **4'** are the first examples of cobalt catalysts active in the hydroboration. Overall, complexes **3**, **3'**, **4**, **4'**, **5** and **5'** complete the small series of catalysts reported for this transformation, based on nickel, ruthenium, iron and copper complexes.^{107,108,113, 118,119} Although the most reactive catalysts in the hydroboration of CO₂ remain based on nickel pincer structures and organic phosphorus bases, the present copper system has a catalytic activity and a selectivity close to (dmpe)₂FeH₂.^{106, 109, 113}

Conclusion

In conclusion, the synthesis and characterization (crystal structure, NMR spectroscopy) of metal complexes of the first row Fe^{2+} , Co^{2+} , and Cu^+ ions have been described with the tripodal ligands $\text{PhSi}(\text{YPPh})_3$ ($\text{Y} = \text{CH}_2$ (**1**), O (**2**)). Replacing the CH_2 group with an O atom affects the coordination properties of the molecule favoring $\kappa^3\text{-PhSi}(\text{OPPh})_3$ versus $\kappa^2\text{-PhSi}(\text{CH}_2\text{PPh})_3$ coordination onto CoCl_2 . All the complexes are active in the catalytic hydroboration of CO_2 with $(9\text{-BBN})_2$. While the $\text{PhSi}(\text{CH}_2\text{PPh})_3$ (**1**) ligand favors the catalytic performances of Fe^{2+} and Co^{2+} ions over its oxygen analogue $\text{PhSi}(\text{OPPh})_3$ (**2**), the reverse trend is observed with the Cu^+ complexes **5** and **5'** which proved the most active catalysts. The activity of the triphosphinite complex **5'** is higher than that of **5**. Both copper catalysts favor the reduction of CO_2 to the C^0 acetal product, and the selective and quantitative conversion of $(9\text{-BBN})_2$ into a 80:20 mixture of $\text{H}_2\text{C}(\text{OBBN})_2$ and CH_3OBBN is obtained at room temperature. The iron and cobalt catalysts are more sluggish and require heating at $60\text{ }^\circ\text{C}$ to perform the hydroboration of CO_2 . They also exhibit a selectivity different from the copper complexes and facilitate the reduction of CO_2 to methoxyboranes, preferentially. The different mechanisms at play in these catalysts classes are currently under scrutiny in our laboratory, to highlight the different active forms of the metal catalysts.

Experimental

The complexes described herein are moisture sensitive. Syntheses and manipulations of the compounds were conducted under ultra-high purity argon atmosphere with rigorous exclusion of air and water (< 5 ppm oxygen or water), using Schlenk-vessel and vacuum-line techniques or in recirculating mBraun LabMaster DP gloveboxes.

Glassware was dried overnight at $70\text{ }^\circ\text{C}$ before use. All NMR spectra were obtained using a Bruker DPX 200 MHz spectrometer. Chemical shifts for ^1H and $^{13}\text{C}\{^1\text{H}\}$ NMR spectra were referenced to solvent impurities. The solvents toluene, pentane, diethyl ether and tetrahydrofuran were dried over a mixture of sodium-benzophenone, and pyridine over potassium and they were distilled immediately before use. Deuterated

solvents (Eurisotop), tetrahydrofuran (d_8 -THF), benzene and toluene were dried over a sodium/benzophenone mixture and acetonitrile (d_3 -MeCN) over KH; they are distilled and kept under argon in the gloves box. The commercially available compounds trichlorophenylsilane, diphenylphosphine oxide were obtained from Aldrich, used as received and stored in the gloves box. The amine NEt_3 (Aldrich) was dried over molecular sieve before use, then distilled under vacuum and kept on 4 Å molecular sieve under inert atmosphere. The metal salts CoCl_2 , CuX ($X = \text{I}, \text{Br}$) and $\text{Fe}(\text{OTf})_2$ ($\text{OTf} = \text{O}_3\text{SCF}_3$) were purchased from Strem or Aldrich, degassed and dried under vacuum for 15h and stored under argon. Synthesis of $\text{PhSi}(\text{CH}_2\text{PPh})_3$ (**1**) (sticky beige solid) has already been reported^{1,25} and the new ligand $\text{PhSi}(\text{OPPh})_3$ was prepared from a derived procedure.^{34, 40}

Synthetic procedures

Synthesis of $\text{PhSi}(\text{OPPh})_3$

$\text{PhSi}(\text{OPPh})_3$ (2) : A 10 mL round-bottom flask was charged with diphenylphosphine oxide (230 mg, 1.1 mmol), NEt_3 (175 μL , 1.2 mmol), PhSiCl_3 (60 μL , 0.37 mmol) and freshly distilled toluene (5 mL) was introduced. After 5 h at room temperature the $[\text{HNEt}_3]\text{Cl}$ salt which deposited from the colorless solution was filtered off on a frit in the gloves box and further washed with 5 mL diethyl ether. The solvents of the combined solutions were evaporated under vacuum affording pure **2**, as a colorless oil, in good yield (228 mg, 88 %).
 ^1H NMR $\delta(d_8\text{-THF})$: 7.63–7.27 (m, 35 H).
 $^{13}\text{C}\{^1\text{H}\}$ NMR $\delta(d_8\text{-THF})$: 144.04 (d, $^1J_{\text{PC}} = 23\text{Hz}$, C_i PPh), 135.17 (s, $C_{m,o}$ SiPh), 131.45 (s, C_p SiPh), 129.70 (s, C_p PPh), 128.46 (s, $C_{m,o}$ SiPh), 130.67–128.46 (m, $C_{m,o}$, PPh). $^{31}\text{P}\{^1\text{H}\}$ NMR $\delta(d_8\text{-THF})$: 100.93.

Synthesis of the complexes

$[\text{Fe}(\text{PhSi}\{\text{CH}_2\text{PPh}_2\}(\text{MeCN})_x)[\text{OTf}]_2$ ($x = 2\text{-}3$) and crystal of **$[\text{Fe}(\text{PhSi}\{\text{CH}_2\text{PPh}_2\}(\text{MeCN})_3)[\text{OTf}]_2$ (3)** : A 25 mL round bottom flask was charged with $\text{Fe}(\text{OTf})_2$ (65 mg, 0.18 mmol) and a solution of **1** (140 mg, 0.20 mmol) in acetonitrile

(10 mL). The red solution was stirred for 24 h at room temperature and the solvent evaporated off. The solid residue was washed with pentane (3 x 5 mL) and dried under vacuum to give $[\text{Fe}(\text{PhSi}\{\text{CH}_2\text{PPh}_2\}_3)(\text{MeCN})_x][\text{OTf}]_2$ ($x = 2-3$) as a red solid (117 mg, 55 %). Dark red crystalline needles of $[\text{Fe}(\text{PhSi}\{\text{CH}_2\text{PPh}_2\}_3)(\text{MeCN})_3][\text{OTf}]_2$ (**3**) were obtained by slow diffusion of diethyl ether into an acetonitrile solution of the isolated product.

^1H NMR $\delta(d_3\text{-acetonitrile})$: 7.80-7.54 (m, 35H), 2.06 (m, 6H), 1.94 (CH₃CN-signals); $^{13}\text{C}\{^1\text{H}\}$ NMR $\delta(d_8\text{-THF})$: 134.53 (s), 134.30 (s), 134.06 (s), 133.81 (s), 131.99 (q, $J = 2.85$ Hz), 131.44 (s), 130.61, 128.87 (q, $J = 3.09$ Hz), 128.60, 5.8 (m, CH₂); $^{31}\text{P}\{^1\text{H}\}$ NMR $\delta(d_3\text{-acetonitrile})$: 30.15 (s). Elemental analysis (%) calc. for C₅₃H₅₀F₆FeN₃O₆P₃S₂Si : C, 53.95; H, 4.27; N, 3.56 and calc. for C₅₁H₄₇F₆FeN₂O₆P₃S₂Si : C, 53.78; H, 4.16; N, 2.46; found :C 53.60 ; H 4.41; N 2.93

$[\text{Fe}(\text{PhSi}\{\text{OPPh}_2\}_3)(\text{MeCN})_x][\text{OTf}]_2$ ($x = 2-3$) and crystals of **$[\text{Fe}(\text{PhSi}\{\text{OPPh}_2\}_3)(\text{MeCN})_3][\text{OTf}]_2$ (**3'**)** : A 25 mL round bottom flask was charged with Fe(OTf)₂ (100 mg, 0.28 mmol) and a solution of **2** (215 mg, 0.30 mmol) in acetonitrile (10 mL). The orange solution was stirred for 24 h at room temperature and the solvent evaporated off. The orange solid residue was successively washed with diethyl ether (3 x 5 mL) and then pentane (3 x 5 mL) and dried under vacuum to yield $[\text{Fe}(\text{PhSi}\{\text{OPPh}_2\}_3)(\text{MeCN})_x][\text{OTf}]_2$ ($x = 2-3$) as an orange solid (172 mg, 52 %). Orange crystals of $[\text{Fe}(\text{PhSi}\{\text{OPPh}_2\}_3)(\text{MeCN})_3][\text{OTf}]_2$ (**3'**) were obtained by slow diffusion of diethyl ether into an acetonitrile solution of the isolated product. ^1H NMR $\delta(d_3\text{-acetonitrile})$: 8.45 (m, 1H), 7.90 (m, 4H), 7.51 (m, 8H), 7.28 (m, 23H), 1.94 (CH₃CN-signals); $^{13}\text{C}\{^1\text{H}\}$ NMR $\delta(d_3\text{-acetonitrile})$: 135.43 (s, *C_{m,o}* SiPh), 134.91 (s, *C_p* SiPh), 133.85 (s, *C_i* SiPh), 133.16 (m, *C_i* PPh), 131.09 (s, *C_p* PPh), 129.51 (d, $J_{\text{PC}} = 7.5$ Hz, *C_{m,o}*, PPh), 129.50 (s, *C_{m,o}*, SiPh), 129.43 (d, $J_{\text{PC}} = 7.5$ Hz, *C_{m,o}*, PPh), 128.70 (d, $J_{\text{PC}} = 7$ Hz, *C_{m,o}*, PPh), 128.63 (d, $J_{\text{PC}} = 7$ Hz, *C_{m,o}*, PPh); $^{31}\text{P}\{^1\text{H}\}$ NMR $\delta(d_3\text{-acetonitrile})$: 147.93 (s). Elemental analysis (%) calc. for C₅₀H₄₄F₆FeN₃O₉P₃S₂Si : C 50.64 ; H 3.74; calc. for C₄₈H₄₁F₆FeN₂O₉P₃S₂Si : C 50.36 ; H 3.61; found C 50.78 ; H 3.54.

[Co(PhSi{CH₂PPh₂})₃Cl₂] (4) : A 25 mL round bottom flask was charged with CoCl₂ (15 mg, 0.12 mmol) and a solution of **1** (100 mg, 0.14 mmol) in 10 mL THF. The resulting blue solution was stirred for 24 h at room temperature. The solvent was evaporated off affording a blue powder which was washed with pentane (3 x 5mL) and then dried under vacuum to yield pure **4** as a blue solid (56 mg, 49%). Blue crystals of **4** were obtained by slow diffusion of pentane into a THF solution of the isolated product.

¹H NMR δ(*d*₂-CH₂Cl₂): 18.15 (s, *W*_{1/2} = 36Hz, 1H), 17.13 (s, *W*_{1/2} = 48Hz, 1H), 13.91 (s, *W*_{1/2} = 63Hz, 18H), 8.37–7.63 (br.m, 15H), 2.33 (s, *W*_{1/2} = 295 Hz, 6H); ¹³C and ³¹P{¹H} NMR: no signals due to the paramagnetic nature of cobalt(II). Elemental analysis (%) calc. for C₄₅H₄₁Cl₂CoP₃Si : C 64.91 ; H 4.96; found: C 64.03 ; H 4.68.

[Co(PhSi{OPPh₂})₃Cl₂] (4') : A 25 mL round bottom flask was charged with blue CoCl₂ (25 mg, 0.20 mmol) and a solution of **2** (165 mg, 0.23 mmol) in 10 mL THF. The resulting deep red solution was stirred for 24 h at room temperature. The solvent was evaporated off affording a red solid which was washed successively with diethyl ether (3 x 5mL) and pentane (3 x 5mL) and then dried under vacuum to give **4'** in moderate yield, as a red solid (60 mg, 36 %). Dark red crystals of **4'** were obtained by slow diffusion of pentane into a dichloromethane solution of the isolated product. ¹H NMR δ(*d*₈-THF): 11.13 (s, *W*_{1/2} = 390Hz, 12H), 7.80–7.19 (m, 23H 23H). ¹³C and ³¹P{¹H} NMR (*d*₈-THF): no signals due to the paramagnetic nature of cobalt(II). Elemental analysis (%) calc. for C₄₂H₃₅Cl₂CoO₃P₃Si: C 60.16 ; H 4.21; found: C 60.12 ; H 4.33.

[Cu(PhSi{CH₂PPh₂})₃Br] (5) : A 25 mL round bottom flask was charged with CuBr (17 mg, 0.12 mmol) and a solution of **1** (100 mg, 0.14 mmol) in 10 mL of THF. The resulting colorless solution was stirred for 24 h at room temperature without change of color. The solution was concentrated to 3 mL and the addition of 6 mL pentane induced precipitation of a white solid of **5** which was isolated pure after filtration and drying under vacuum (77 mg, 76 %). Colorless crystals of the solvate **5**·(THF)₃ were obtained by diffusion of pentane into a THF solution of the product.

^1H NMR $\delta(d_2\text{-CH}_2\text{Cl}_2)$: 7.67–7.08 (m, 35H), 1.71 (s, 6H); $^{13}\text{C}\{^1\text{H}\}$ NMR $\delta(\text{CH}_2\text{Cl}_2\text{-}d_2)$: 136.99 (br.s, $W_{1/2} = 30\text{Hz}$, Ci PPh), 136.19 (d, $J_{\text{PC}} = 7\text{Hz}$, Ci SiPh), 133.37 (s, Cm,o SiPh), 131.54 (d, $J_{\text{PC}} = 11\text{Hz}$, Cm,o , PPh), 131.44 (d, $J_{\text{PC}} = 11\text{Hz}$, Cm,o , PPh), 130.40 (s, Cp SiPh), 129.30 (s, Cp PPh), 128.48 (s, Cm,o SiPh), 128.39 (d, $J_{\text{PC}} = 6.3\text{Hz}$, Cm,o , PPh), 128.33 (d, $J_{\text{PC}} = 6.3\text{Hz}$, Cm,o , PPh), 8.33 (s, CH₂); $^{31}\text{P}\{^1\text{H}\}$ NMR $\delta(d_2\text{-CH}_2\text{Cl}_2)$: -33 (m, $J_{\text{P-}^{63}\text{Cu}} \sim 840\text{ Hz}$, $J_{\text{P-}^{65}\text{Cu}} \sim 900\text{ Hz}$). Elemental analysis (%) calc. for $\text{C}_{45}\text{H}_{41}\text{BrCuP}_3\text{Si}$: C 63.87 ; H 4.88; found: C 64.03 ; H 4.39.

[Cu(PhSi(OPPh₂)₃)Br] (5'') : A 25 mL round bottom flask was charged with CuBr (20 mg, 0.14 mmol) and a solution of **2** (110 mg, 0.15 mmol) in 10 mL THF. The initially colorless solution was stirred for 24 h at room temperature without change of color. The solution was concentrated to 3 mL and the addition of 6 mL pentane induced precipitation of a white solid of **5''** which was isolated pure after filtration and drying under vacuum (98 mg, 82 %). Colorless crystals of the solvate **5''**·(THF) were obtained by diffusion of pentane into a THF solution of the product.

^1H NMR $\delta(d_8\text{-THF})$: 8.05–8.02 (m, 2H), 7.69–7.57 (m, 17H), 7.13–7.02 (m, 16H); $^{31}\text{P}\{^1\text{H}\}$ NMR $\delta(d_8\text{-THF})$: 81 (very broad singlet); $\delta(\text{C}_6\text{D}_6)$: 82.9 (very broad singlet); Elemental analysis (%) calc. for $\text{C}_{42}\text{H}_{35}\text{CuBrO}_3\text{P}_3\text{Si}$: C 59.20 ; H 4.14; found: C 60.67; H 4.79.

[Cu(PhSi(OPPh₂)₃)I] (5') : A 25 mL round bottom flask was charged with CuI (30 mg, 0.16 mmol) and a solution of **2** (150 mg, 0.21 mmol) in 10 mL THF. The initially colorless solution was stirred for 24 h at room temperature without change of color. The solution was concentrated to 3 mL and the addition of 6 mL pentane induced precipitation of a white solid of **5'** which was isolated pure after filtration and drying under vacuum (125 mg, 88 %). Colorless crystals of the solvate **5'**·(THF) were obtained by diffusion of pentane into a THF solution of the product.

^1H NMR $\delta(d_2\text{-CH}_2\text{Cl}_2)$: 8.02–7.99 (m, 2H), 7.70–7.49 (m, 17H), 7.19–7.03 (m, 16H); $^{13}\text{C}\{^1\text{H}\}$ NMR $\delta(d_2\text{-CH}_2\text{Cl}_2)$: 137.72 (br.s, $W_{1/2} = 33\text{ Hz}$, Ci PPh), 134.42 (s, Cm,o SiPh), 128.57 (s, Cm,o SiPh), 132.64 (s, Cp SiPh), 130.16 (s, Cp PPh), 129.34 (d, $J_{\text{PC}} =$

13Hz, *Cm,o*, PPh) et 129.20 (d, $J_{PC} = 13\text{Hz}$, *Cm,o*, PPh), 128.27(d, $J_{PC} = 6.9\text{Hz}$, *Cm,o*, PPh) et 128.21 (d, $J_{PC} = 6.9\text{Hz}$, *Cm,o*, PPh), 126.27 (s, *Ci* SiPh); $^{31}\text{P}\{^1\text{H}\}$ NMR δ (d_2 -CH₂Cl₂): 80 (m, $J_{P-Cu} \sim 860$ Hz).

Crystals of the solvate compound [Cu₂(Ph₂POPPh₂)₂(NCMe)₂](MeCN) (6·MeCN)
: In an NMR tube, CuI (10 mg, 0.05 mmol) and **2** (37mg, 0.05 mmol) were charged in 0.5 mL acetonitrile. The suspension, kept at room temperature for 24 h and heated at 80°C for 2 h, afforded a colorless solution. Colorless crystalline blocks of **6**·MeCN were obtained by slow diffusion of diethyl ether into the solution.

Crystals of [Cu(Ph₃Si₃O₃{OPPh₂})₃Cl] (7) : In a NMR tube, CuCl₂ (9.4 mg, 0.07 mmol) and **2** (271 μL , 0.07 mmol) were charged in 0.5 mL of THF. The suspension was heated at reflux for 15 h. Colorless crystals of the reduced complex **7** were obtained by diffusion of pentane into the THF.

Catalytic experiments

Catalytic reactions have been performed in a J-Young NMR tube equipped with valve. In an NMR tube, the borane (9-BBN)₂ (ca 0.09 or 0.20mmole) and the catalyst (1.5 mol%) were weighted and dissolved in 0.4 mL of d_3 -acetonitrile, then 7 μL (0.05 mmol) of mesitylene were added. The tube was then fitted onto a vacuum line, degassed under vacuum after having freeze the solution and filled with 1 atmosphere of pure CO₂ (quality 4.5, ca 0.08 mmole).

Crystallography

The data were collected at 150(2) K on a Nonius Kappa-CCD area detector diffractometer¹²⁰ using graphite-monochromated Mo-K α radiation ($\lambda = 0.71073$ Å). The crystals were introduced into glass capillaries with a protective coating of Paratone-N oil (Hampton Research). The unit cell parameters were determined from ten frames, then refined on all data. The data (combinations of φ - and ω -scans with a minimum redundancy of at least 4 for 90% of the reflections) were processed with HKL2000.¹²¹ Absorption effects were corrected empirically with the program SCALEPACK.¹²¹ The structures were solved by intrinsic phasing with SHELXT¹²² expanded by subsequent

difference Fourier synthesis and refined by full-matrix least-squares on F^2 with SHELXL-2014.¹²³⁻¹²⁴ All non-hydrogen atoms were refined with anisotropic displacement parameters.

In compound **3**, one of the trifluoromethanesulfonate counter-ions is disordered over two positions sharing two oxygen and two fluorine atoms, which were refined with occupancy parameters constrained to sum to unity and restraints on bond lengths and displacement parameters.

In compound **4**, the displacement parameters of several carbon atoms in the phenyl rings are highly anisotropic, which is probably indicative of unresolved disorder.

In compound **4'**, the phenyl ring bound to Si1 is rotationally disordered over two positions sharing two carbon atoms, which were refined with occupancy parameters constrained to sum to unity; one of these positions (A) was refined as an idealized hexagon and the other (B) with restraints on bond lengths and angles.

Complex **5**·3THF was refined as a two-component inversion twin, with a Flack parameter of 0.479(13).

In compound **7**, some voids in the lattice indicate the presence of unresolved solvent molecules, but, the residual electronic density in these voids being quite low, the SQUEEZE software (PLATON)¹²⁵ did not improve the data significantly. These solvent molecules may have at least partially left the lattice, as suggested by the partly opaque aspect of all crystals.

In all compounds, the hydrogen atoms were introduced at calculated positions and they were treated as riding atoms with an isotropic displacement parameter equal to 1.2 times that of the parent atom (1.5 for CH₃, with optimized geometry). Crystal data and structure refinement parameters are given in Table 3. The molecular plots were drawn with ORTEP-3.¹²⁶

Acknowledgments

This work was supported financially by the CEA, CNRS, CHARMMMAT Laboratory of Excellence, and the European Research Council (ERC starting grant agreement no. 336467). T.C. thanks the Foundation Louis D.-Institut de France for its support. The authors thank Dr. Emmanuel Nicolas for fruitful discussions regarding NMR spectroscopy.

Captions to Figures

Scheme 1: Synthesis of the PhSi(XPPh₂)₃ ligands (X = O, CH₂).

Scheme 2: Synthesis of the Fe²⁺, Co²⁺ and Cu⁺ complexes with the PhSi(YPPh₂)₃ ligands (Y = O, CH₂).

Scheme 3: Complexes 6 and 7 obtained from degradation of ligand 2

Figure 1. Views of complexes **3** (left) and **3'** (right). Displacement ellipsoids are drawn at the 30% probability level. The counterions and hydrogen atoms are omitted.

Figure 2. Views of complexes **4** (left) and **4'** (right). Displacement ellipsoids are drawn respectively at the 30% and 40% probability level. The hydrogen atoms are omitted. For **4'** only one position of the disordered aromatic ring is represented

Figure 3. ³¹P{¹H} NMR spectra of **5** (left) and **5'** (right) in *d*₂-CH₂Cl₂ at 21°C

Figure 4. Views of complexes **5** (left) and **5'** (right). Displacement ellipsoids are drawn at the 30% probability level. The solvent molecules and hydrogen atoms are omitted.

Figure 5. View of complex **6**. Displacement ellipsoids are drawn at the 50% probability level. The solvent molecule and hydrogen atoms are omitted. Symmetry code: $i = 1 - x, y, 3/2 - z$.

Figure 6. View of complex **7**. Displacement ellipsoids are drawn at the 30% probability level. The hydrogen atoms are omitted. Symmetry codes: $i = z, x, y; j = y, z, x$.

Table 1. Selected bond lengths (Å) and angles (°) in the complexes **3**, **3'** and **4**, **4'**

3		3'		4		4'	
Distances							
Fe1–N1	1.963(4)	Fe1–N1	1.967(2)	Co1–Cl1	2.2318(10)	Co1–Cl1	2.2600(8)
Fe1–N2	1.953(4)	Fe1–N2	1.958(2)	Co1–Cl2	2.2061(10)	Co1–Cl2	2.2418(8)
Fe1–N3	1.958(3)	Fe1–N3	1.9624(18)	Co1–P1	2.3476(10)	Co1–P1	2.2755(8)
Fe1–P1	2.3031(12)	Fe1–P1	2.2452(6)	Co1–P2	2.3489(10)	Co1–P2	2.1893(8)
Fe1–P2	2.3224(11)	Fe1–P2	2.2532(6)	< Co1–P>	2.3483(6)	Co1–P3	2.2070(8)
Fe1–P3	2.2972(12)	Fe1–P3	2.2656(6)	<P–C>	1.827(13)	< Co1–P>	2.22(4)
<Fe–P>	2.308(11)	<Fe–P>	2.255(8)	<Si–C>	1.881(16)	<P–O>	1.640(4)
<Fe–N>	1.958(4)	<Fe–N>	1.962(4)	Si1–C40	1.866(4)	<Si–O>	1.6402(2)
<P–C>	1.833(8)	<P–O>	1.625(6)			Si1–C37	1.8244(19)
<Si–C>	1.871(13)	<Si1–O>	1.6409(3)				
Si1–C40	1.855(4)	Si1–C37	1.816(2)				
Angles							
N2–Fe1–N3	83.22(14)	N2–Fe1–N3	85.43(7)	Cl1–Co1–Cl2	121.73(4)	Cl1–Co1–Cl2	88.69(3)
N2–Fe1–N1	85.75(14)	N2–Fe1–N1	88.19(8)	P1–Co1–P2	104.27(3)	P2–Co1–P3	92.84(3)
N3–Fe1–N1	86.84(13)	N3–Fe1–N1	85.06(7)			P2–Co1–P1	92.42(3)
P3–Fe1–P2	93.07(4)	P3–Fe1–P2	93.47(2)			P3–Co1–P1	94.56(3)
P1–Fe1–P2	91.61(4)	P1–Fe1–P3	89.12(2)			<P–Co–P>	93.3(9)
P3–Fe1–P1	93.53(4)	P1–Fe1–P2	90.67(2)				
<P–Fe–P>	92.7(8)	<P–Fe–P>	91(2)				

Table 2. Selected bond lengths (Å) and angles (°) in the copper complexes **5-3THF**, **5'-THF**, **6-MeCN** and **7**

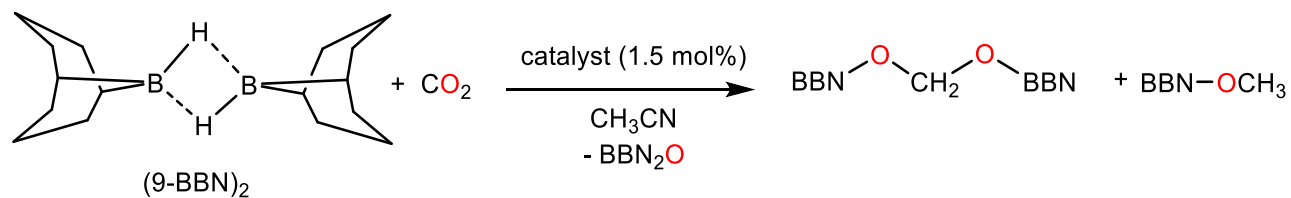
5-3THF		5'-THF		6-MeCN		7	
Distances							
Cu1–Br1	2.4137(12)	Cu1–I1	2.5491(3)	Cu1–I1	2.6937(3)	Cu1–Cl1	2.3022(15)
Cu1–P1	2.287(2)	Cu1–P2	2.2777(7)	Cu1–I1 ⁱ	2.7074(3)	Cu1–P1	2.2550(8)
Cu1–P2	2.280(2)	Cu1–P1	2.2783(6)	Cu1–P1	2.2079(6)	P1–O1	1.623(2)
Cu1–P3	2.289(2)	Cu1–P3	2.2728(7)	Cu1–N1	1.973(2)	P1–C13	1.819(3)
<Cu–P>	2.285(4)	<Cu–P>	2.276(2)	Cu1–Cu1 ⁱ	2.8024(5)	Si1–O1	1.626(2)
<P–C>	1.832(7)	<P–C>	1.809(2)	P1–O1	1.6498(12)	Si1–C1	1.833(3)
<Si–C>	1.886(14)	Si1–C37	1.829(2)	<P1–C(Ph)>	1.8165(15)	<Si–O2>	1.6355(15)
Si1–C40	1.863(8)						
Angles							
P1–Cu1–P2	98.85(8)	P3–Cu1–P2	96.64(2)	I1–Cu1–I1 ⁱ	109.697(10)	P1–Cu1–Cl1	105.08(3)
P2–Cu1–P3	101.38(8)	P3–Cu1–P1	96.43(2)	N1–Cu1–P1	124.59(6)	P1–Cu1–P1 ⁱ	113.48(2)
P1–Cu1–P3	101.46(8)	P2–Cu1–P1	96.57(2)	N1–Cu1–I1	106.81(6)		
P2–Cu1–Br1	114.58(6)	P3–Cu1–I1	122.43(2)	N1–Cu1–I1 ⁱ	104.75(6)		
P1–Cu1–Br1	120.54(7)	P2–Cu1–I1	120.858(19)	P1–Cu1–I1	106.114(18)		
P3–Cu1–Br1	116.84(6)	P1–Cu1–I1	118.109(18)	P1–Cu1–I1 ⁱ	104.369(17)		
<P–Co–P>	100.6(12)	<P–Co–P>	96.55(9)	O1–P1–C7	100.77(9)		
				O1–P1–C1	100.28(8)		
				O1–P1–Cu1	116.33(7)		
				P1–O1–P1 ⁱ	124.31(14)		

Table 3. Crystal data and structure refinement details

	3	3'	4	4'
Chemical formula	C ₅₃ H ₅₀ F ₆ FeN ₃ O ₆ P ₃ S ₂ Si	C ₅₀ H ₄₄ F ₆ FeN ₃ O ₉ P ₃ S ₂ Si	C ₄₅ H ₄₁ Cl ₂ CoP ₃ Si	C ₄₂ H ₃₅ Cl ₂ CoO ₃ P ₃ Si
<i>M</i> /g mol ⁻¹	1179.93	1185.85	832.61	838.53
Crystal system	Triclinic	Monoclinic	Monoclinic	Monoclinic
Space group	<i>P</i> $\bar{1}$	<i>P</i> 2 ₁ / <i>c</i>	<i>P</i> 2 ₁ / <i>n</i>	<i>P</i> 2 ₁ / <i>c</i>
<i>a</i> /Å	13.8465(10)	13.2856(5)	13.5425(9)	9.8162(3)
<i>b</i> /Å	14.2314(8)	23.6456(9)	13.5858(5)	20.6578(7)
<i>c</i> /Å	15.3249(12)	17.1543(4)	24.5419(17)	19.1760(7)
α /°	73.403(5)	90	90	90
β /°	79.675(4)	102.994(2)	105.036(4)	101.210(2)
γ /°	70.236(4)	90	90	90
<i>V</i> /Å ³	2712.1(3)	5251.0(3)	4360.8(5)	3814.3(2)
<i>Z</i>	2	4	4	4
<i>D</i> _{calcd} /g cm ⁻³	1.445	1.500	1.268	1.460
μ (Mo K α)/mm ⁻¹	0.538	0.560	0.683	0.787
<i>F</i> (000)	1216	2432	1724	1724
Reflections collected	117414	194968	121962	128536
Independent reflections	10290	9959	8275	7220
Observed reflections [<i>I</i> > 2 σ (<i>I</i>)]	6157	8074	5168	5649
<i>R</i> _{int}	0.073	0.024	0.058	0.047
Parameters refined	716	679	469	494
<i>R</i> ₁	0.057	0.037	0.051	0.039
<i>wR</i> ₂	0.153	0.095	0.112	0.106
<i>S</i>	1.090	1.026	0.983	1.132
$\Delta\rho_{\min}$ /e Å ⁻³	-0.75	-0.48	-0.40	-0.81
$\Delta\rho_{\max}$ /e Å ⁻³	2.10	0.40	0.54	0.76

	5·3THF	5'·THF	6·MeCN	7
Chemical formula	C ₅₇ H ₆₅ BrCuO ₃ P ₃ Si	C ₄₆ H ₄₃ CuIO ₄ P ₃ Si	C ₃₂ H ₃₂ Cu ₂ I ₂ N ₄ OP ₂	C ₅₄ H ₄₅ ClCuO ₆ P ₃ Si ₃
<i>M</i> /g mol ⁻¹	1062.54	971.24	931.43	1066.07
Crystal system	Monoclinic	Orthorhombic	Monoclinic	Cubic
Space group	<i>Pn</i>	<i>Pbca</i>	<i>C2/c</i>	<i>Pa-3</i>
<i>a</i> /Å	10.2468(8)	19.0061(3)	22.3076(10)	22.2970(4)
<i>b</i> /Å	14.6429(11)	21.5469(5)	8.4153(3)	22.2970(4)
<i>c</i> /Å	17.7472(7)	21.4927(5)	21.1830(10)	22.2970(4)
α /°	90	90	90	90
β /°	97.487(4)	90	118.621(2)	90
γ /°	90	90	90	90
<i>V</i> /Å ³	2640.1(3)	8801.8(3)	3490.7(3)	11085.1(6)
<i>Z</i>	2	8	4	8
<i>D</i> _{calcd} /g cm ⁻³	1.337	1.466	1.772	1.278
μ (Mo K α)/mm ⁻¹	1.327	1.376	3.110	0.640
<i>F</i> (000)	1108	3936	1816	4400
Reflections collected	87659	284218	60399	119259
Independent reflections	9799	11344	5263	3506
Observed reflections [<i>I</i> > 2 σ (<i>I</i>)]	8535	8933	4550	2617
<i>R</i> _{int}	0.101	0.016	0.045	0.027
Parameters refined	596	505	197	205
<i>R</i> ₁	0.060	0.035	0.032	0.047
<i>wR</i> ₂	0.161	0.098	0.086	0.130
<i>S</i>	1.070	1.061	1.064	1.099
$\Delta\rho_{\min}$ /e Å ⁻³	-0.47	-0.74	-1.00	-0.37
$\Delta\rho_{\max}$ /e Å ⁻³	0.72	1.02	1.08	0.32

Table 4. Catalytic hydroboration of CO₂ with complexes **3,3'**, **4, 4'** and **5, 5'** as depicted in the equation below.



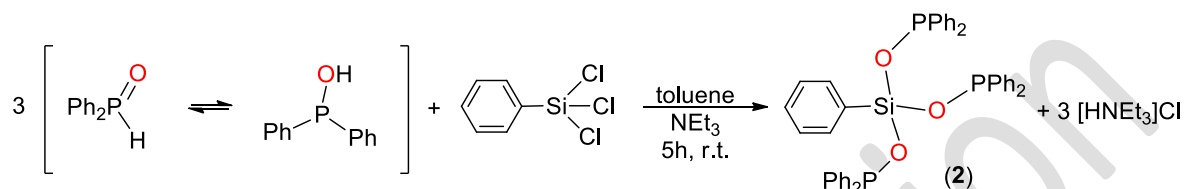
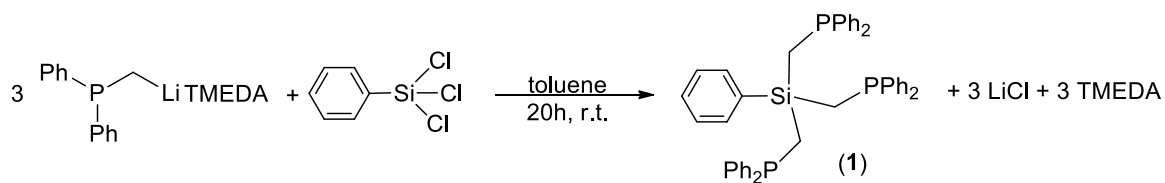
Entry	Catalyst (1.5 mol%) ^b	Borane ^a (0.18 mmol of B-H)	T (°C)	Reaction time (h)	Selectivity ^c (acetal/methoxy)	Conversion (%) ^b	TON ^d	TOF(h ⁻¹) ^e
1	-	(9-BBN) ₂	r.t.	> 48	-	No conversion ¹¹⁰		
2	5 (Cu)	(9-BBN) ₂	r.t.	4	69 :31	8	5	1.3
3	5 (Cu)	(9-BBN) ₂	r.t.	24	71:29	45	30	1.3
4	5' (Cu)	(9-BBN) ₂	r.t.	4	92:8	69	46	11.5
5	5' (Cu)	(9-BBN) ₂	r.t.	24	80:20	99	66	2.8
6	5 (Cu)	(9-BBN) ₂	60	4	41:59	57	38	9.5
7	5 (Cu)	(9-BBN) ₂	60	24	24:76	94	63	2.6
8	5' (Cu)	(9-BBN) ₂	60	4	30:70	88	59	14.8
9	5' (Cu)	(9-BBN) ₂	60	24	6:94	99	66	2.8
10	3 (Fe)	(9-BBN) ₂	60	24	19:81	45	30	1.3
11	3 (Fe)	(9-BBN) ₂	60	40	15:85	51	34	0.9
12	3' (Fe)	(9-BBN) ₂	60	24	0:100	3	2	0.1
13	3' (Fe)	(9-BBN) ₂	60	40	0:100	10	7	0.2
14	4 (Co)	(9-BBN) ₂	60	24	61:39	63	42	1.8
15	4 (Co)	9-BBN	60	40	21:79	63	42	1
16	4' (Co)	(9-BBN) ₂	60	24	0:100	6	4	0.2
17	4' (Co)	(9-BBN) ₂	60	40	0:100	6	4	0.1
Entry	Catalyst (1.5 mol%) ^b	Borane (0.4 mmol of B-H)	T (°C)	Reaction time (h)	Selectivity ^c (acetal:methoxy)	Conversion (%) ^b	TON	TOF(h ⁻¹) ^e
18	-	(9-BBN) ₂	r.t.	> 48	-	No conversion ¹¹⁰		
19	5' (Cu)	(9-BBN) ₂	r.t.	7	86:14	17	11	1.6
20	3 (Fe)	(9-BBN) ₂	60	24	5:95	75	50	2.1
21	3 (Fe)	(9-BBN) ₂	60	40	0:100	99	66	1.7
22	4 (Co)	(9-BBN) ₂	60	24	8:92	99	66	2.8

23	4 (Co)	(9-BBN) ₂	60	40	0:100	99	66	1.7
----	--------	----------------------	----	----	-------	----	----	-----

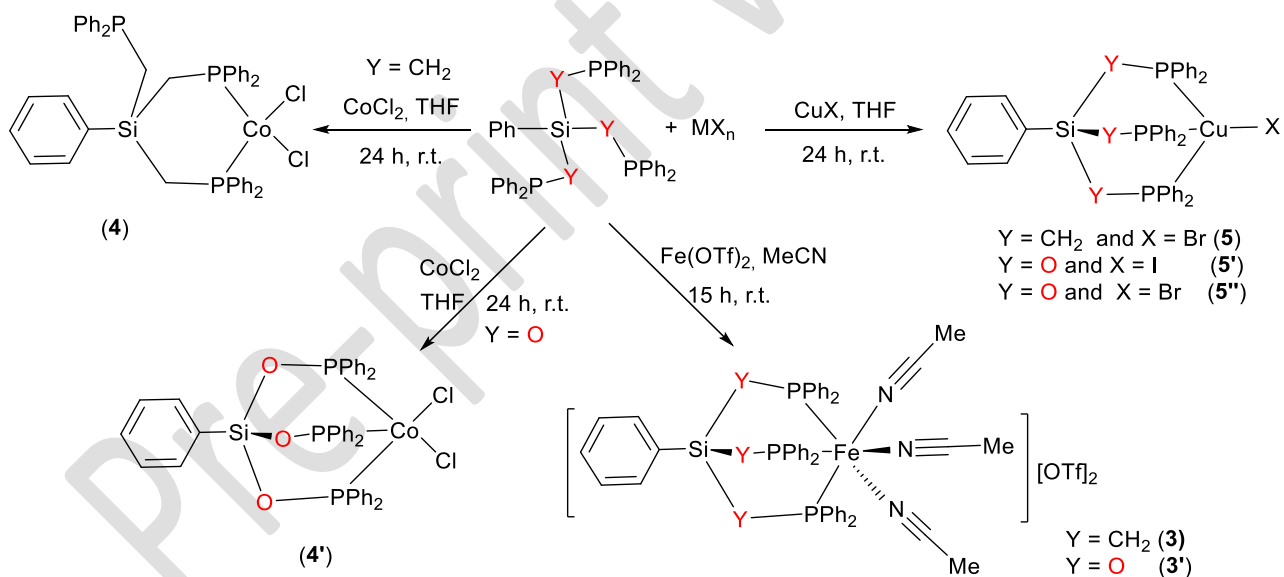
Reaction conditions : a) 0.18 mmol of B-H functionalities (0.09 mol of (9-BBN)₂); b) % calculated relatively to the quantity of B-H functionalities; c) Yields and selectivity determined by ¹H NMR using mesitylene as internal standard; d) TON = [mmol(acetal) x 2 + mmol(methoxy) x 3]/mmol catalyst; e) TOF = TON/time(h).

Pre-print version

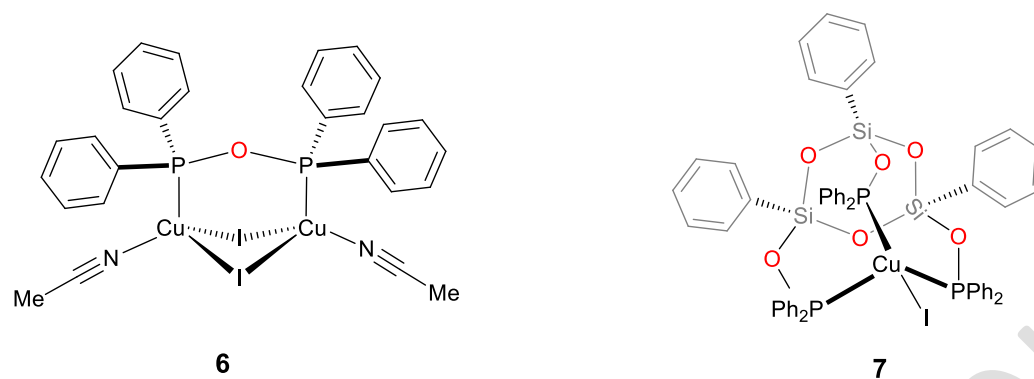
Scheme 1.



Scheme 2.



Scheme 3.



Pre-print version

Figure 1.

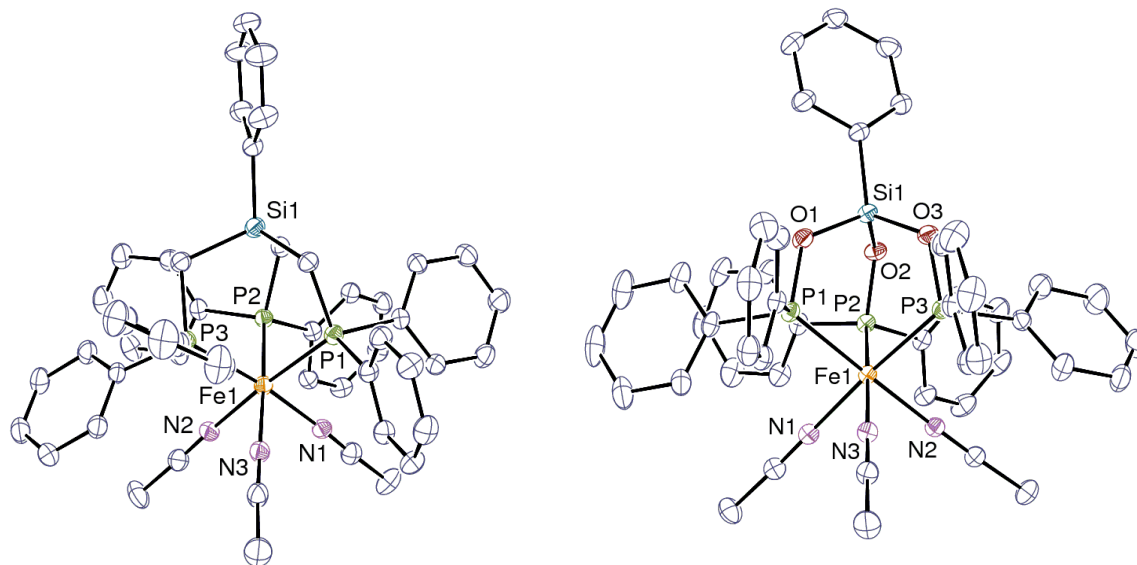


Figure 2.

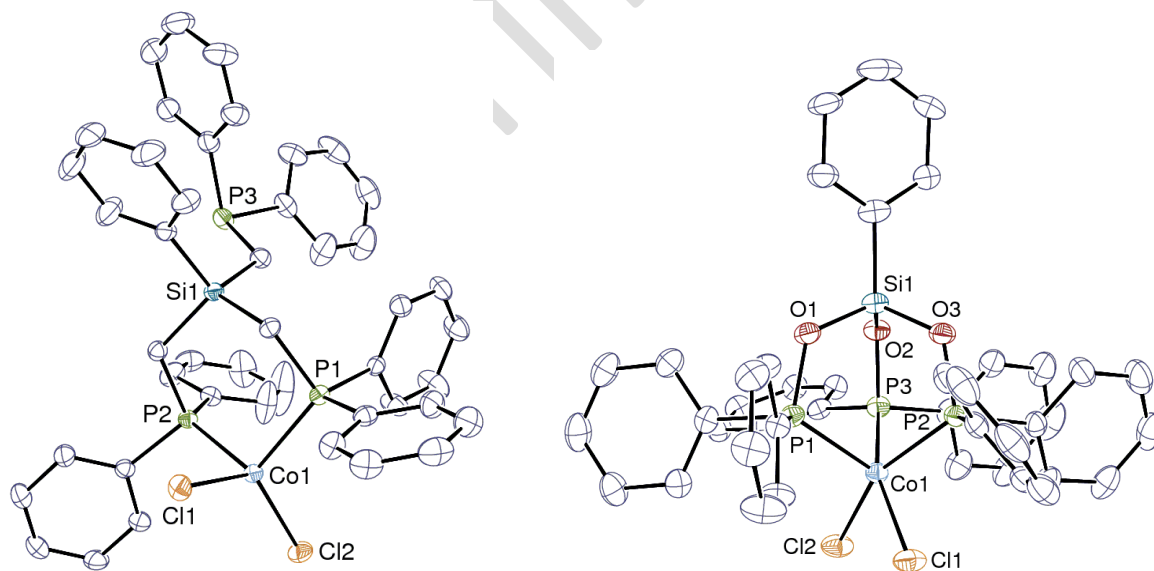


Figure 3.

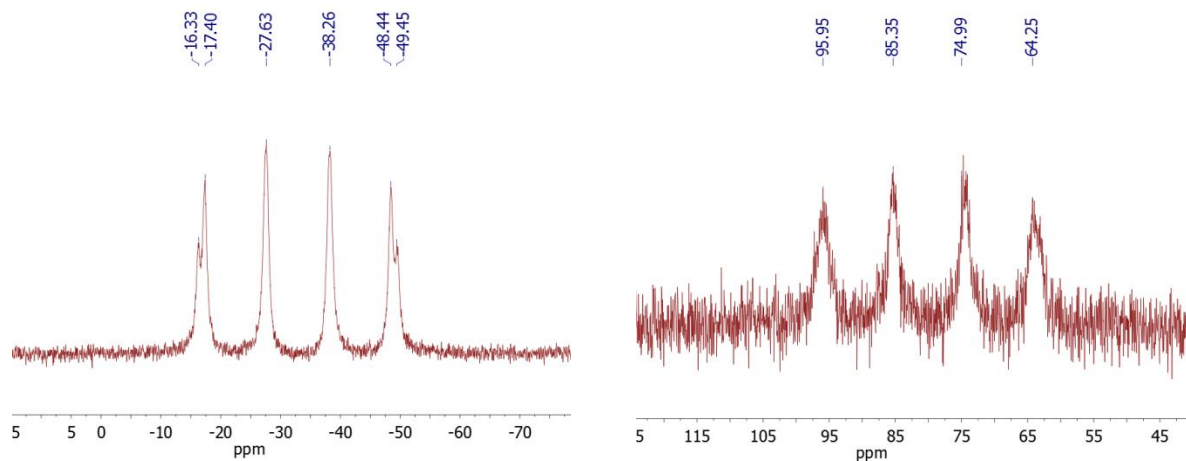


Figure 4.

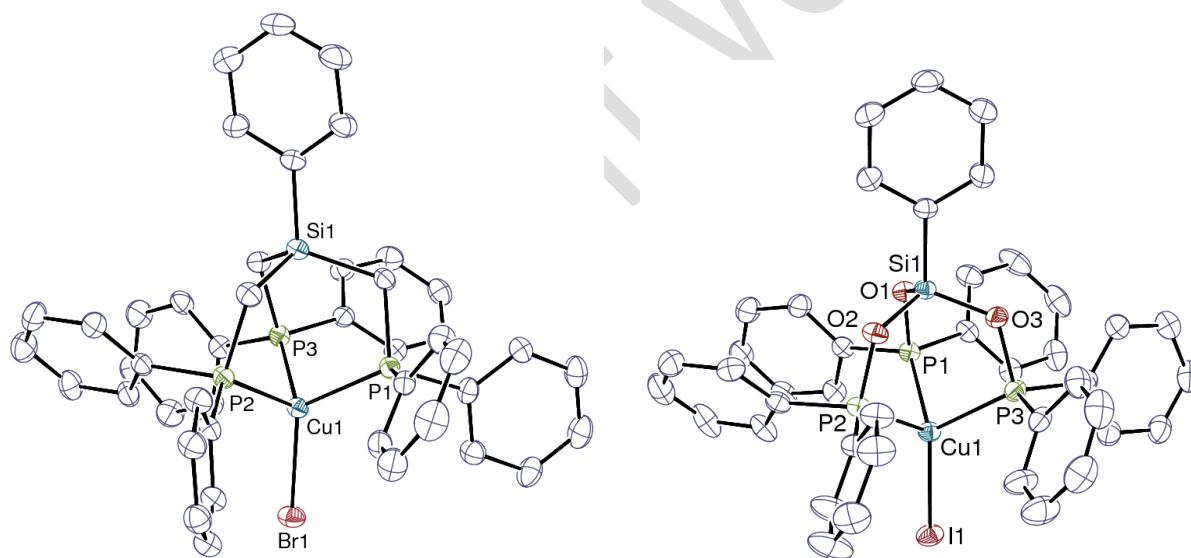


Figure 5.

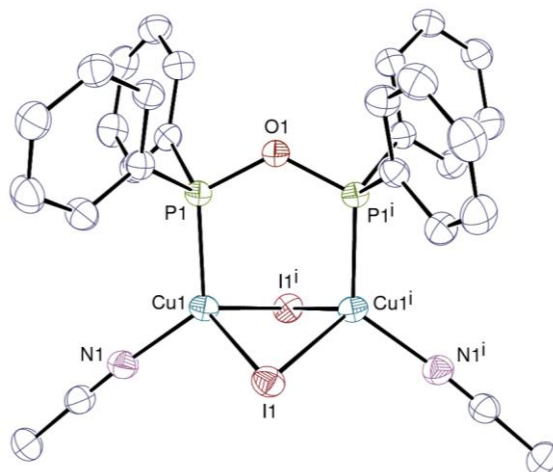
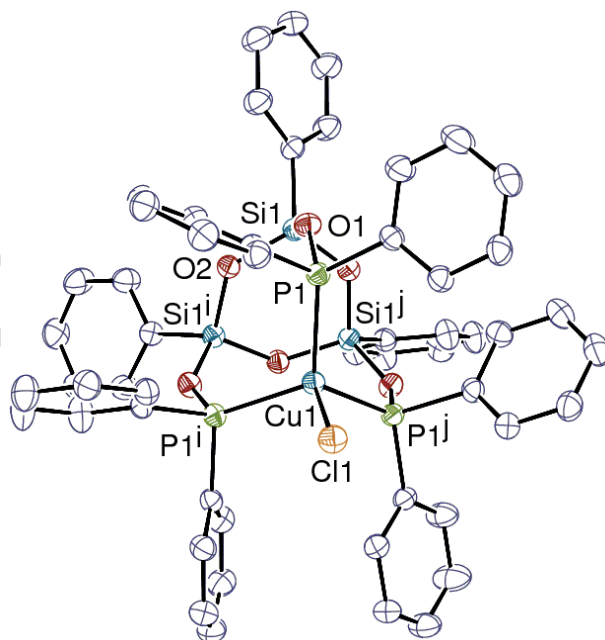


Figure 6.



References

1. F. Neumeyer, M. I. Lipschutz and T. D. Tilley, *Eur. J. Inorg. Chem.*, 2013, **2013**, 6075-6078.
2. J. C. Hierso, R. Amardeil, E. Bentabet, R. Broussier, B. Gautheron, P. Meunier and P. Kalck, *Coord. Chem. Rev.*, 2003, **236**, 143-206.
3. H. A. Mayer and W. C. Kaska, *Chem. Rev.*, 1994, **94**, 1239-1272.
4. F. A. Cotton, Hong, B., *Prog. Inorg. Chem.*, 1992, **40**, 179-289.
5. M. Meuresch, S. Westhues, W. Leitner and J. Klankermayer, *Angew. Chem. Int. Ed.*, 2016, **55**, 1392-1395.
6. S. Wesselbaum, T. vom Stein, J. Klankermayer and W. Leitner, *Angew. Chem. Int. Ed.*, 2012, **51**, 7499-7502.
7. S. Savourey, G. Lefevre, J. C. Berthet, P. Thuéry, C. Genre and T. Cantat, *Angew. Chem. Int. Ed.*, 2014, **53**, 10466-10470.
8. A. Phanopoulos, A. J. P. White, N. J. Long and P. W. Miller, *Acs Catalysis*, 2015, **5**, 2500-2512.
9. T. vom Stein, M. Meuresch, D. Limper, M. Schmitz, M. Holscher, J. Coetzee, D. J. Cole-Hamilton, J. Klankermayer and W. Leitner, *J. Am. Chem. Soc.*, 2014, **136**, 13217-13225.
10. C. Bianchini, C. A. Ghilardi, A. Meli, S. Midollini and A. Orlandini, *Inorg. Chem.*, 1985, **24**, 924-931.
11. Y. J. You and G. S. Girolami, *Organometallics*, 2008, **27**, 3172-3180.
12. Y. J. You, S. R. Wilson and G. S. Girolami, *Organometallics*, 1994, **13**, 4655-4657.
13. T. G. Gardner and G. S. Girolami, *Organometallics*, 1987, **6**, 2551-2556.
14. T. G. Gardner and G. S. Girolami, *Angew. Chem. Int. Ed.*, 1988, **27**, 1693-1695.
15. T. W. Hayton, P. Legzdins and B. O. Patrick, *Inorg. Chem.*, 2002, **41**, 5388-5396.
16. T. W. Hayton, P. J. Daff, P. Legzdins, S. J. Rettig and B. O. Patrick, *Inorg. Chem.*, 2002, **41**, 4114-4126.
17. T. W. Hayton, B. O. Patrick and P. Legzdins, *Organometallics*, 2004, **23**, 657-664.
18. T. G. Gardner and G. S. Girolami, *J. Chem. Soc., Chem. Commun.*, 1987, 1758-1760.
19. J. M. Boncella, M. L. H. Green and D. Ohare, *J. Chem. Soc., Chem. Commun.*, 1986, 618-619.
20. J. M. Boncella and M. L. H. Green, *J. Organomet. Chem.*, 1987, **325**, 217-231.
21. A. Petuker, K. Merz, C. Merten and U. P. Apfel, *Inorg. Chem.*, 2016, **55**, 1183-1191.
22. K. A. Thoreson, A. D. Follett and K. McNeill, *Inorg. Chem.*, 2010, **49**, 3942-3949.
23. K. A. Thoreson and K. McNeill, *Dalton Trans.*, 2011, **40**, 1646-1648.
24. M. F. Cain, D. S. Glueck, J. A. Golen and A. L. Rheingold, *Organometallics*, 2012, **31**, 775-778.
25. M. L. H. Green, D. Ohare and J. G. Watkin, *J. Chem. Soc., Chem. Commun.*, 1989, 698-701.
26. H. Broda, S. Hinrichsen, J. Krahmer, C. Nather and F. Tuczek, *Dalton Trans.*, 2014, **43**, 2007-2012.
27. H. Broda, J. Krahmer and F. Tuczek, *Eur. J. Inorg. Chem.*, 2014, 3564-3571.
28. K. McNeill, R. A. Andersen and R. G. Bergman, *J. Am. Chem. Soc.*, 1995, **117**, 3625-3626.
29. K. McNeill, R. A. Andersen and R. G. Bergman, *J. Am. Chem. Soc.*, 1997, **119**, 11244-11254.
30. A. W. Holland and R. G. Bergman, *Organometallics*, 2002, **21**, 2149-2152.
31. L. Dahlenburg, S. Kerstan and D. Werner, *J. Organomet. Chem.*, 1991, **411**, 457-469.
32. P. J. Daff, P. Legzdins and S. J. Rettig, *J. Am. Chem. Soc.*, 1998, **120**, 2688-2689.
33. M. Bogza, T. Oeser and J. Blumel, *J. Organomet. Chem.*, 2005, **690**, 3383-3389.
34. N. Greene, H. Taylor, T. P. Kee and M. Thorntonpett, *J. Chem. Soc., Dalton Trans.*, 1993, 821-825.
35. Q. Liu, L. P. Wu, R. Jackstell and M. Beller, *Nature Comm.*, 2015, **6**.
36. M. Aresta, *Carbon Dioxide as Chemical Feedstock* Wiley-VCH, Weinheim, 2010.
37. H. H. Karsch and A. Appelt, *Z. Naturforsch., B: Chem. Sci.*, 1983, **38**, 1399-1405.
38. T. R. Ward, L. M. Venanzi, A. Albinati, F. Lianza, T. Gerfin, V. Gramlich and G. M. R. Tombo, *Helv. Chim. Acta*, 1991, **74**, 983-988.

39. K. Issleib and B. Walther, *J. Organomet. Chem.*, 1970, **22**, 375-&.
40. N. Greene and T. P. Kee, *Polyhedron*, 1993, **12**, 2471-2475.
41. G. V. Goeden, J. C. Huffman and K. G. Caulton, *Inorg. Chem.*, 1986, **25**, 2483-2485.
42. A. Asam, B. Janssen, G. Huttner, L. Zsolnai and O. Walter, *Z. Naturforsch., B: Chem. Sci.*, 1993, **48**, 1707-1714.
43. H. Heidel, J. Scherer, A. Asam, G. Huttner, O. Walter and L. Zsolnai, *Chem. Ber.*, 1995, **128**, 293-301.
44. B. J. A. Asam, G. Huttner, L. Zsolnai, O. Walter, *Z. Naturforsch.*, 1993, **48b**, 1707

45. K. Heinze, G. Huttner, L. Zsolnai and P. Schober, *Inorg. Chem.*, 1997, **36**, 5457-5469.
46. D. F. Dempsey and G. S. Girolami, *Organometallics*, 1988, **7**, 1208-1213.
47. H. G. Yu, X. Z. Tan, G. M. Bernard, V. V. Terskikh, J. L. Chen and R. E. Wasylshen, *J. Phys. Chem. A*, 2015, **119**, 8279-8293.
48. E. H. Wong, L. Prasad, E. J. Gabe and F. C. Bradley, *J. Organomet. Chem.*, 1982, **236**, 321-331.
49. A. D. Burrows, M. F. Mahon, M. T. Palmer and M. Varrone, *Inorg. Chem.*, 2002, **41**, 1695-1697.
50. J. Bravo, J. Castro, S. Garcia-Fontan, M. C. Rodriguez-Martinez and P. Rodriguez-Seoane, *Eur. J. Inorg. Chem.*, 2006, 3028-3040.
51. I. Ara, J. Fornies, S. Ibanez, P. Mastrorilli, S. Todisco and V. Gallo, *Dalton Trans.*, 2016, **45**, 2156-2171.
52. B. Hoge and B. Kurscheid, *Angew. Chem. Int. Ed.*, 2008, **47**, 6814-6816.
53. D. J. Irvine, C. Glidewell, D. J. Colehamilton, J. C. Barnes and A. Howie, *J. Chem. Soc., Dalton Trans.*, 1991, 1765-1772.
54. Y. L. Zhao, Y. B. Zhou, T. Q. Chen, S. F. Yin and L. B. Han, *Inorg. Chim. Acta*, 2014, **422**, 36-39.
55. Y. B. Zhou, S. F. Yin, Y. X. Gao, Y. F. Zhao, M. Goto and L. B. Han, *Angew. Chem. Int. Ed.*, 2010, **49**, 6852-6855.
56. S. Pavlik, K. Mereiter, M. Puchberger and K. Kirchner, *J. Organomet. Chem.*, 2005, **690**, 5497-5507.
57. R. Kruszynski and W. Wiczorek, *Acta Crystallogr. Sect. E: Struct. Rep. Online*, 2001, **57**, o624-o626.
58. M. P. Castaldi, S. E. Gibson, M. Rudd and A. J. P. White, *Chem. Eur. J.*, 2006, **12**, 138-148.
59. S. M. F. Vilela, A. D. G. Firmino, R. F. Mendes, J. A. Fernandes, D. Ananias, A. A. Valente, H. Ott, L. D. Carlos, J. Rocha, J. P. C. Tome and F. A. A. Paz, *Chem. Commun.*, 2013, **49**, 6400-6402.
60. J. Zon, D. Y. Kong, K. Gagnon, H. Perry, L. Holliness and A. Clearfield, *Dalton Trans.*, 2010, **39**, 11008-11018.
61. R. Murugavel and M. P. Singh, *New J. Chem.*, 2010, **34**, 1846-1854.
62. M. P. Castaldi, S. E. Gibson, M. Rudd and A. J. P. White, *Angew. Chem. Int. Ed.*, 2005, **44**, 3432-3435.
63. S. M. F. Vilela, J. A. Fernandes, D. Ananias, L. D. Carlos, J. Rocha, J. P. C. Tome and F. A. A. Paz, *Cryst. Eng. Comm.*, 2014, **16**, 344-358.
64. P. Garczarek, J. Janczak, M. Duczmal and J. Zon, *Polyhedron*, 2014, **81**, 132-141.
65. M. I. Garcia-Seijo, P. Sevillano, R. O. Gould, D. Fernandez-Anca and M. E. Garcia-Fernandez, *Inorg. Chim. Acta*, 2003, **353**, 206-216.
66. D. K. Srivastava, N. P. Rath and L. Barton, *Polyhedron*, 1992, **11**, 1251-1259.
67. P. Comba, C. Katsichtis, B. Nuber and H. Pritzkow, *Eur. J. Inorg. Chem.*, 1999, 777-783.
68. C. W. R. D. Pike, *private communication*, CCDC ref code UMOCAA01, 2013.
69. B. Punji, J. T. Mague, S. M. Mobin and M. S. Balakrishna, *Polyhedron*, 2009, **28**, 101-106.
70. S. Sculfort, P. Croizat, A. Messaoudi, M. Benard, M. M. Rohmer, R. Welter and P. Braunstein, *Angew. Chem. Int. Ed.*, 2009, **48**, 9663-9667.

71. A. Bondi, *J. Phys. Chem.*, 1964, **68**, 441-&.
72. W. F. Fu, X. Gan, C. M. Che, Q. Y. Cao, Z. Y. Zhou and N. N. Y. Zhu, *Chem. Eur. J.*, 2004, **10**, 2228-2236.
73. A. M. James, A. W. Maverick and F. R. Fronczek, *Private Communication*, CCDC 1042173 code ref LOVDAD, 2015.
74. S. Naik, M. Kumaravel, J. T. Mague and M. S. Balakrishna, *Dalton Trans.*, 2014, **43**, 1082-1095.
75. D. J. Fife, H. J. Mueh and C. F. Campana, *Acta Crystallogr. Sect. C: Cryst. Struct. Commun.*, 1993, **49**, 1714-1716.
76. K. Foltling, J. Huffman, W. Mahoney, J. M. Stryker and K. G. Caulton, *Acta Crystallogr. Sect. C: Cryst. Struct. Commun.*, 1987, **43**, 1490-1492.
77. M. Aresta, A. Dibenedetto and A. Angelini, *Chem. Rev.*, 2014, **114**, 1709-1742.
78. M. Aresta and A. Dibenedetto, *Dalton Trans.*, 2007, 2975-2992.
79. C. D. Gomes, O. Jacquet, C. Villiers, P. Thuéry, M. Ephritikhine and T. Cantat, *Angew. Chem. Int. Ed.*, 2012, **51**, 187-190.
80. N. MacDowell, N. Florin, A. Buchard, J. Hallett, A. Galindo, G. Jackson, C. S. Adjiman, C. K. Williams, N. Shah and P. Fennell, *Energy Environ. Sci.*, 2010, **3**, 1645-1669.
81. C. Romain and C. K. Williams, *Acs Sym Ser*, 2015, **1192**, 135-146.
82. S. Sopena, G. Fiorani, C. Martin and A. W. Kleij, *Chemsuschem*, 2015, **8**, 3248-3254.
83. K. Nakano, T. Kamada and K. Nozaki, *Angew. Chem. Int. Ed.*, 2006, **45**, 7274-7277.
84. K. Nakano, S. Hashimoto, M. Nakamura, T. Kamada and K. Nozaki, *Angew. Chem. Int. Ed.*, 2011, **50**, 4868-4871.
85. M. North and R. Pasquale, *Angew. Chem. Int. Ed.*, 2009, **48**, 2946-2948.
86. N. Yi, J. Unruangsri, J. Shaw and C. K. Williams, *Faraday Discuss.*, 2015, **183**, 67-82.
87. E. A. Quadrelli, G. Centi, J. L. Duplan and S. Perathoner, *Chemsuschem*, 2011, **4**, 1194-1215.
88. W. Wang, S. P. Wang, X. B. Ma and J. L. Gong, *Chem. Soc. Rev.*, 2011, **40**, 3703-3727.
89. C. Oloman and H. Li, *Chemsuschem*, 2008, **1**, 385-391.
90. J. M. Savéant, *Chem. Rev.*, 2008, **108**, 2348-2378.
91. A. A. Peterson and J. K. Nørskov, *J. Phys. Chem.*, 2012, **3**, 251-258.
92. E. E. Benson, C. P. Kubiak, A. J. Sathrum and J. M. Smieja, *Chem. Soc. Rev.*, 2009, **38**, 89-99.
93. C. Costentin, S. Drouet, M. Robert and J. M. Savéant, *Science*, 2012, **338**, 90-94.
94. C. A. Huff and M. S. Sanford, *J. Am. Chem. Soc.*, 2011, **133**, 18122-18125.
95. P. G. Jessop, T. Ikariya and R. Noyori, *Chem. Rev.*, 1995, **95**, 259-272.
96. S. Wesselbaum, V. Moha, M. Meuresch, S. Brosinski, K. M. Thenert, J. Kothe, T. V. Stein, U. Englert, M. Holscher, J. Klankermayer and W. Leitner, *Chem. Sci.*, 2015, **6**, 693-704.
97. P. G. Jessop, F. Joo and C. C. Tai, *Coord. Chem. Rev.*, 2004, **248**, 2425-2442.
98. S. Bontemps, *Coord. Chem. Rev.*, 2016, **308**, 117-130.
99. S. N. Riduan, Y. G. Zhang and J. Y. Ying, *Angew. Chem. Int. Ed.*, 2009, **48**, 3322-3325.
100. A. Berkefeld, W. E. Piers, M. Parvez, L. Castro, L. Maron and O. Eisenstein, *Chem. Sci.*, 2013, **4**, 2152-2162.
101. M. Khandelwal and R. J. Wehmschulte, *Angew. Chem. Int. Ed.*, 2012, **51**, 7323-7326.
102. S. Park, D. Bezier and M. Brookhart, *J. Am. Chem. Soc.*, 2012, **134**, 11404-11407.
103. H. Koinuma, F. Kawakami, H. Kato and H. Hirai, *J. Chem. Soc., Chem. Commun.*, 1981, 213-214.
104. A. Berkefeld, W. E. Piers and M. Parvez, *J. Am. Chem. Soc.*, 2010, **132**, 10660-10661.
105. W. Sattler and G. Parkin, *J. Am. Chem. Soc.*, 2012, **134**, 17462-17465.
106. M. A. Courtemanche, M. A. Legare, L. Maron and F. G. Fontaine, *J. Am. Chem. Soc.*, 2013, **135**, 9326-9329.
107. S. Bontemps, L. Vendier and S. Sabo-Etienne, *Angew. Chem. Int. Ed.*, 2012, **51**, 1671-1674.
108. S. Chakraborty, J. Zhang, J. A. Krause and H. R. Guan, *J. Am. Chem. Soc.*, 2010, **132**, 8872-8873.

109. E. Blondiaux, J. Pouessel and T. Cantat, *Angew. Chem. Int. Ed.*, 2014, **53**, 12186-12190.
110. C. D. Gomes, E. Blondiaux, P. Thuéry and T. Cantat, *Chem. Eur. J.*, 2014, **20**, 7098-7106.
111. A. Tlili, E. Blondiaux, X. Frogneux and T. Cantat, *Green Chem.*, 2015, **17**, 157-168.
112. X. Frogneux, E. Blondiaux, P. Thuéry and T. Cantat, *Acs Catalysis*, 2015, **5**, 3983-3987.
113. G. H. Jin, C. G. Werncke, Y. Escudié, S. Sabo-Etienne and S. Bontemps, *J. Am. Chem. Soc.*, 2015, **137**, 9563-9566.
114. D. Wang and D. Astruc, *Chem. Rev.*, 2015, **115**, 6621-6686.
115. D. Mellmann, E. Barsch, M. Bauer, K. Grabow, A. Boddien, A. Kammer, P. Sponholz, U. Bentrup, R. Jackstell, H. Junge, G. Laurency, R. Ludwig and M. Beller, *Chem. Eur. J.*, 2014, **20**, 13589-13602.
116. A. Boddien, D. Mellmann, F. Gartner, R. Jackstell, H. Junge, P. J. Dyson, G. Laurency, R. Ludwig and M. Beller, *Science*, 2011, **333**, 1733-1736.
117. P. S. D. Mellmann, H. Junge and M. Beller, *Chem. Soc. Rev.*, 2016, DOI: [10.1039/c5cs00618j](https://doi.org/10.1039/c5cs00618j).
118. R. Shintani and K. Nozaki, *Organometallics*, 2013, **32**, 2459-2462.
119. M. J. Sgro and D. W. Stephan, *Angew. Chem. Int. Ed.*, 2012, **51**, 11343-11345.
120. R. W. W. Hooft, *COLLECT; Nonius BV: Delft, The Netherlands*, 1998.
121. Z. Otwinowski and W. Minor, *Methods Enzymol.*, 1997, **276**, 307.
122. G. M. Sheldrick, *Acta Crystallogr. Sect. A*, 2015, **71**, 3-8.
123. G. M. Sheldrick, *Acta Crystallogr. Sect. C*, 2015, **71**, 3-8.
124. G. M. Sheldrick, *Acta Crystallogr. Sect. A*, 2008, **64**, 112-122.
125. A. L. Spek, *J. Appl. Crystallogr.*, 2003, **36**, 7.
126. L. J. Farrugia, *J. Appl. Crystallogr.*, 1997, **30**, 565.